Time-dependent pair cascades in magnetospheres of neutron stars – I. Dynamics of the polar cap cascade with no particle supply from the neutron star surface

A. N. Timokhin[1,2]★

[1]*Astronomy Department, University of California at Berkeley, 601 Campbell Hall, Berkeley, CA 94720, USA*
[2]*Sternberg Astronomical Institute, Universitetskij pr. 13, Moscow 119992, Russia*

ABSTRACT

I argue that the problem of electromagnetically driven electron–positron cascades in magnetospheres of neutron stars must be addressed starting from first principles. I describe a general numerical algorithm for doing self-consistent kinetic simulations of electron–positron cascades – wherein particle acceleration, pair creation and screening of the electric field are calculated simultaneously – and apply it to model the Ruderman & Sutherland cascade in one dimension. I find that pair creation is quite regular and quasi-periodic. In each cycle a blob of ultra-relativistic electron–positron plasma is generated; it propagates into the magnetosphere leaving a tail of less relativistic plasma behind, and the next discharge occurs when this mildly relativistic plasma leaves the polar cap. A short burst of pair formation is followed by a longer quiet phase when accelerating electric field is screened and no pairs are produced. Some of freshly injected electron–positrons pairs get trapped in plasma oscillations creating a population of low-energy particles. The cascade easily adjusts to the current density required by the pulsar magnetosphere by reversing some of the low-energy particles. Each discharge generates a strong coherent superluminal electrostatic wave, which may be relevant for the problem of pulsar radioemission.

Key words: acceleration of particles – plasmas – stars: magnetic field – stars: neutron – pulsars: general.

1 INTRODUCTION

Rotation-powered pulsars remain a profound puzzle despite the fact that the first pulsar was discovered 40 yr ago (Hewish et al. 1968). A pulsar is a rapidly rotating, strongly magnetized neutron star (NS), as it was originally proposed by Gold (1969) and Pacini (1967), with most of its radiation produced in the magnetosphere. However, there is still no consistent quantitative pulsar model. Proposed models range from a NS with charge-starved electrosphere (Krause-Polstorff & Michel 1985) to a NS with force-free magnetosphere, where acceleration of particles and, hence, emitting zones are localized in very small spatial regions (Goldreich & Julian 1969).

The force-free magnetosphere model is favoured by the majority of astrophysicists working on pulsars. There are observational hints favouring this model: (i) young pulsars produce relativistic winds with particle number density much larger than it is necessary to screen accelerating electric field parallel to the magnetic field; (ii) pulse peaks are narrow, what points to smallness of emitting regions,

and, hence, to smallness of regions where particles are accelerated. From theoretical point of view, as it was pointed out by Sturrock (1971), physical conditions in the polar cap of pulsar are almost ideal for generation of electron–positron pair plasma. The energy density of the generated plasma is negligible compared to the energy density of the magnetic field near the NS. The magnetosphere, if filled with plasma, almost certainly being force-free (almost everywhere) near the NS should be force-free at much larger scales as well; at least numerical simulations of the force-free magnetosphere of an aligned rotator have shown that magnetosphere can remain force-free up to distances much larger than the light cylinder radius (Timokhin 2006).

Therefore, pursuing the force-free model as a 'standard model' seems to be reasonable. Recently the force-free pulsar magnetosphere model has been studied in great detail (e.g. Contopoulos, Kazanas & Fendt 1999; Gruzinov 2005; Timokhin 2006, 2007a; Spitkovsky 2006; Kalapotharakos & Contopoulos 2009; Bai & Spitkovsky 2010). The force-free magnetosphere is a restricted magnetohydrodynamic system which does not admit any current density distribution. By fixing the boundary conditions – in the case of a pulsar these are the variation of accelerating potential across

★E-mail: atimokhin@berkeley.edu

the polar cap and the size of the corotating zone – one fixes the current density distribution. It turns out that the admitted range of current density distributions in the force-free magnetosphere with realistic boundary conditions – when the potential drop in the polar cap is less than a vacuum one – is rather limited (Timokhin 2006, 2007a,b). For young pulsars, where potential drop in the polar cap must be small, the current density is not constant and strongly deviates from the Goldreich–Julian (GJ) current density $j_{GJ} \equiv \eta_{GJ} c$ (η_{GJ} is the GJ charge density and c is the speed of light); along some magnetic field lines it has the sign opposite to the sign of the GJ charge density.

Pair production in the polar cap of pulsar is vital for sustaining of the force-free magnetosphere – without it there will be not enough plasma to cancel the accelerating electric field. Currents flowing in the open field line zone of the magnetosphere flow through the pair-producing region at the base of the polar cap; therefore, any model of the polar cap cascade zone must agree with a global magnetosphere model on the current density flowing along magnetic field lines. Many previously proposed models for polar cap cascades (and almost all quantitative models) assumed stationary unidirectional outflow of a charge separated particle beam (e.g. Arons & Scharlemann 1979; Daugherty & Harding 1982; Muslimov & Tsygan 1992; Harding & Muslimov 2002; Hibschman & Arons 2001a). All these models predicted current density being almost equal to the GJ current density everywhere in the polar cap of pulsar. This prediction is in strong disagreement with the force-free magnetosphere model: for young pulsars like Crab a deviation of the charge density from η_{GJ} of the order of few per cents – and in unidirectional flow this implies the same deviation of the current density from j_{GJ} – can account for all pulsar emission. Both sides of this discrepancy are based on detailed simulations and it is not possible to change some parameters in order to fit the models together. So, either the *magnetosphere* is non-force-free or non-stationary (or both) or *polar cap cascades* do not operate according to the existing models.

From the energetic point of view a stationary (on the rotation time-scale) force-free configuration seems to be the most preferable state of the magnetosphere. The inductance of the magnetosphere is much larger than that of the polar cap, therefore, the current density in the polar cap will be set by the magnetosphere and not in the opposite way (e.g. Mestel 1999). In my opinion these are strong hints that existing quantitative models for particle acceleration and pair production in pulsar polar cap do not work. Particle acceleration and electron–positron pair production in cascade zones can be essentially non-stationary: time intervals of effective particle acceleration could alternate with intervals when the accelerating electric field is screened by electron–positron pairs created in the cascade; in fact, in the first paper on pulsar cascades (Sturrock 1971) the particle flow was assumed to be non-stationary. The current density flowing through non-stationary cascade fluctuates strongly and the amplitude of the fluctuation should depend on the microphysics of the pair-generation process, not on the global physics of the magnetosphere. However, the characteristic time-scale of polar cap cascades (microseconds) is much shorter than the magnetospheric time-scale (longer than milliseconds) so that all fluctuations due to cascade non-stationarity will be washed out. The average current density in the cascade zone could be adjusted to the current density required by the magnetosphere by adjusting the time cascade spent in 'active' and 'passive' phases. On the other hand, it is still possible that particle flow in the cascade zone is nevertheless stationary but not unidirectional – with some particles trapped in a non-trivial accelerating potential (Arons 2009). However, all these qualitative statements have to be proved.

Electromagnetically driven electron–positron cascades can operate not only in polar caps of radiopulsars. Some pulsars in outer parts of their magnetospheres – close to the place where the GJ charge density changes the sign – could have so-called 'outer-gap' cascade zones (Cheng, Ruderman & Sutherland 1976); although it seems that such acceleration zone can exist only if polar cap cascades fail to supply enough pair plasma to short-out the electric field in the entire magnetosphere. Electromagnetically driven cascades should generate plasma in magnetospheres of magnetars along open (Thompson 2008) as well as closed magnetic field lines (Beloborodov & Thompson 2007). Electron–positron cascades can also work in magnetospheres of black holes (Beskin, Istomin & Parev 1992). The study of pair cascade dynamics is, therefore, of significance for a broad class of astrophysical problems.

Non-stationary regime of electromagnetically driven cascades is poorly investigated. Only few attempts have been made before to construct quantitative models for non-stationary cascades. Al'Ber, Krotova & Eidman (1975) were the first, their model was 0D – it accounted only for variability in time. It predicted strong time variability in pair creation rate due to the delay between emission of a high-energy photon and its decay into an electron–positron pair. Fawley (1978) tried to make a numerical model for Ruderman & Sutherland (1975) cascade using 1D particle-in-cell (PIC) code and a simple version of on-the-spot approximation for pair injection. At that time it was a formidable numerical problem; simulations could be performed only for a very short time after cascade ignition, so that no conclusive results could be drawn from them. Levinson et al. (2005), Luo & Melrose (2008), Melrose, Rafat & Luo (2009) used 1D two-fluid approximation for electron–positron plasma and on-the-spot approximation for pair injection; they studied polar cap cascades operating in the space charge limited flow regime and found that generation of pairs is essentially turbulent – pair were created throughout all physical region admitting pair creation. Beloborodov & Thompson (2007) studied pair cascades in the closed field line zone of magnetar magnetosphere. They used on-the-spot approximation for pair injection and tracked motion of electrons and positrons in self-consistently calculated electric field; the electric field was assumed to be zero at both ends of the field line. They too concluded that pair creation is turbulent.

In all of these models some or other simplifying assumptions about physical processes at play were used. It is difficult to draw decisive conclusions about the character of particle flow pattern from them because it is not clear a priori whether ignoring one of the aspect of cascade physics can result in qualitatively different behaviour or not. In my view, the study of electron–positron cascades should be done starting *ab initio*. No assumptions about the character of particle flow should be made and the key 'ingredients' of the system must be preserved in the model: back reaction of particles on the accelerating electric field and the delay between photon emission and pair injection. Possible complexity of system behaviour compels to conduct a numerical experiment where particle acceleration, pair production and variation in the accelerating electric field are modelled self-consistently.

With this paper, I intend to start a series of publications dedicated to self-consistent numerical modelling of full kinetics of electron–positron pair cascades in magnetospheres of NSs. In this paper I describe a numerical algorithm for self-consistent modelling of electromagnetic cascades starting from first principles and apply it for study of the most simple model of polar cap cascade – when particles cannot escape the NS surface – the Ruderman & Sutherland (1975) model. The goal of this work is not merely to quantify the Ruderman–Sutherland model but to try to infer basic properties of

electromagnetic cascades. The most important qualitative questions about basic cascade properties I try to answer are (i) what is the character of plasma flow and (ii) how the pair cascade adjusts to the current density required by the magnetosphere.

The structure of the paper is as follows. In Section 2, I describe the general numerical algorithm I developed for modelling of electromagnetic cascades. In Section 3, I describe physical and numerical aspects of the polar cap cascade model. Simulations results and their analysis are presented in Section 4; I summarize the inferred cascade properties in Section 4.6. In Section 5, I discuss limitations of the model, applicability of physical approximations used in previous works and implication of the results for physics of radiopulsars.

2 GENERAL NUMERICAL ALGORITHM

In electromagnetically driven pair cascade in NS magnetosphere the following physical processes determine the behaviour of the system.

(i) Charged particles – electrons and positrons – are accelerated by the electric field induced by NS rotation.

(ii) Particles emit high-energy gamma-rays. The radiation mechanisms relevant for pulsars include curvature radiation, inverse Compton scattering (in both resonant and non-resonant regime) of thermal X-ray photons emitted by the NS, and synchrotron radiation of freshly created pairs (e.g. Sturner, Dermer & Michel 1995; Zhang & Harding 2000).

(iii) Gamma photons propagate some distance and then create electron–positron pairs. In pulsar polar cap the dominating process is the single photon pair creation in the strong magnetic field (Sturrock 1971). In the outer pulsar magnetosphere, the dominant process will be photon–photon pair creation either on soft photons emitted by the NS (thermal X-rays) or on soft photons produced in the cascade itself (Cheng, Ho & Ruderman 1986).

(iv) Creation of electron–positron pairs increases plasma density and changes the electric field: if a pair is created in a region with strong electric field, electron and positron are accelerated in opposite directions and redistribution of the charge density alters the accelerating electric field.

Probably the best numerical technique for self-consistent modelling of plasma kinetics – acceleration of charged particles and changes of electromagnetic fields induced by their motion [Items (i) and (iv) in the list] – is Particle-In-Cell (e.g. Birdsall & Langdon 1985). There particle distribution is modelled directly by representing plasma by an ensemble of macroparticles. PIC is a mature numerical technique. Many of its properties are well known and are the subject of constant ongoing investigations (e.g. Verboncoeur 2005). Although on the current stage of the project 1D modelling is used, PIC allows straightforward generalization for multi-dimension. Particle emission and creation of electron–positrons pairs – a radiation transfer problem [Items (ii) and (iii)] – in a system with strongly and rapidly changing particle energy distribution are best to model utilizing the Monte Carlo technique (e.g. Sobol' 1973; Fishman 1996); the computational costs of Monte Carlo are almost the same for 1D and multi-dimensional cases. On the other hand, in PIC plasma is already represented by discrete particles, which makes Monte Carlo a natural choice. For modelling of pair cascades I decided to develop a new hybrid PIC/Monte Carlo code. The existing hybrid codes used for modelling of gas discharges do not include radiation transfer and account only for interaction between charged and neutral particles; the Monte Carlo technique there is used to account for interaction randomness.

The mean-free path of gamma-photons does not depend on the plasma density in the polar cap; it is set by the strength of the magnetic field and by the curvature of magnetic field lines. For the minimum mean-free path of photons, the estimate of Ruderman & Sutherland (1975) can be used, which gives $\lambda_{\text{mfp}} \sim 10^3$ cm. In space charge limited flow models photon mean-free path could be comparable to the NS radius, $\lambda_{\text{mfp}} \sim 10^6$ cm. Characteristic plasma scales are of the order of the Debye length which depend on plasma density. A rough estimate for the Debye length can be made assuming plasma density being equal to the GJ number density $n_{\text{GJ}} = \eta_{\text{GJ}}/e$:

$$\lambda_{\text{D}}^{\text{GJ}} \sim \frac{c}{\omega_p^{\text{GJ}}} = c \left(\frac{4\pi\eta_{\text{GJ}}e}{m_{\text{e}}} \right)^{-1/2} \simeq 2 B_{12}^{-1/2} P^{-1/2} \,\text{cm}\,, \qquad (1)$$

where B_{12} is the pulsar magnetic field in units of 10^{12} G and P is the pulsar period in seconds. The photon mean-free path is much larger than the Debye length, and so it sets the macroscopic scale – the length of the computational domain. The Debye length of the plasma sets the microscopic scale of computations – the cell size. It will be unwise to advance photons in space at the same pace as particles – photons propagate large distance to the absorption point without interaction while particle motion can change on very small spatial scales. Propagation of photons must be calculated separately, with larger spatial steps.

For modelling of electromagnetic cascades in NS magnetospheres I developed a general algorithm which calculates plasma motion and photon propagation in different numerical pace. The scheme of the algorithm is presented in Fig. 1, where the sequence of operations performed at every time-step is shown.

The plasma dynamics is done with the standard PIC algorithm. Using the current density known from the previous step I solve Maxwell equations and get electric field at grid points. Then for each particle I interpolate the electric field to the particle's position and get the electric force on the particle. Solving the equation of motion I advance particle momenta and positions. Particle motion through the cell boundary is counted as its contribution to the electric current. The electric current for each cell boundary is computed simultaneously with particle motion and is stored for the next time-step.

Photon emission and pair production are calculated as follows. I sample how many photons capable of producing electron–positron pair each particle emits during the current time-step. For each emitted photon, its energy is sampled from the spectral energy distribution of the corresponding emission process. Then I sample the distance the photon will travel until it is absorbed. Calculation of the optical depth to pair creation is done with the space steps adjusted according to the current value of the cross-section for photon absorption; most of the steps are much larger that the cell size. In this way photon propagation is done in (appropriate) and much faster numerical pace than particle advance. Photon's energy, position and time of absorption are stored in an array. At every time-step I iterate over the photon array and pick up photons which are absorbed at the current time-step. For each of the selected photons I inject an electron and a positron at the point of photon absorption and delete that photon from the array. Being injected at the same point freshly created electron and positron do not contribute to the charge and current densities at the time-step of injection.

If there are too many particles of a particular kind in the computational domain, their number can be reduced by deleting some randomly selected particles. The total statistical weight of the selected particles is stored and then statistical weights of all remaining particles of the same kind are increased in order to compensate for
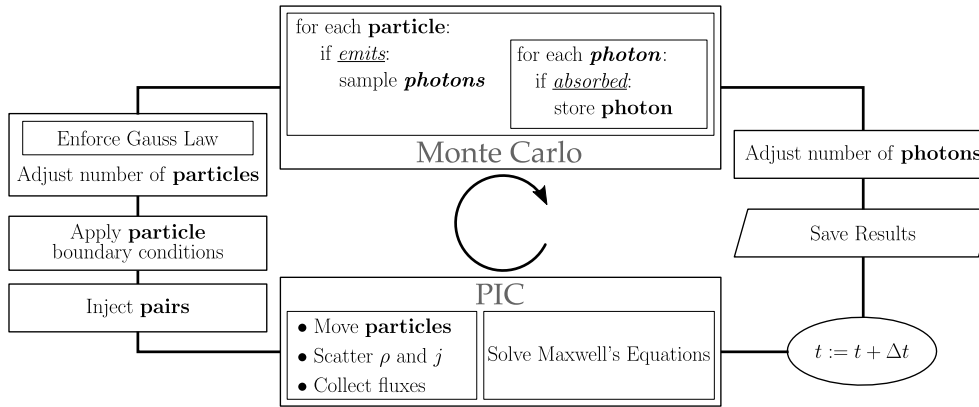
Figure 1. Code structure – sequence of operations performed at every time-step.

the deleted particles. Although this conserves the overall charge of the system, the resulting charge distribution will be slightly different from the one before particle deletion. To proceed with charge conserving algorithm one needs to solve the Poisson equation in order to bring the electric field in accordance with the altered charge distribution. When the number of photons is reduced, the later step is, of course, unnecessary.

3 ONE-DIMENSIONAL DISCHARGE IN PULSAR POLAR CAP

As previously there were no truly self-consistent studies of electromagnetic cascades – allowing time-dependence and incorporating all classes of relevant microscopic processes – I decided to address first the simplest case in order to develop an intuition about physics of pair plasma generation. It was not clear a priori what is the pattern of plasma flow, and in order to develop an appropriate numerical technique to model a realistic system with many microscopic processes at play a 'bare-bone' model must be studied first.

3.1 Physical model

The Ruderman & Sutherland (1975) model for pair cascade in the polar cap of pulsar is the simplest possible model for a pair cascade. Ruderman and Sutherland considered the case when the NS angular velocity is anti-parallel to its magnetic momentum – so that the GJ charge density is positive – and assumed that the work function to extract a positive ion from the surface of an NS is much larger than the available electric potential. In this model there is no plasma inflow from the surface of the NS and all plasma in the cascade zone is produced by pair creation in a series of 'discharges'. When enough plasma is produced in the discharge zone, it screens the accelerating electric field and, therefore, stops particle acceleration and pair creation. Plasma flows into the magnetosphere and – as there is no source of plasma than (now suppressed) pair creation – the plasma density decreases. When there are not enough charged particles to screen the accelerating electric field the pair formation starts again.

Although there are hints (e.g. Medin & Lai 2007) that the work function in the NS crust can be small enough – so that particles can be extracted from the star – and cascade operates in the so-called space-charge limited flow regime (Arons & Scharlemann 1979), I think that studying of the Ruderman–Sutherland model is worth the effort. As reasons for this I give the following points: (i) this model is intrinsically non-stationary and should be a good test of

whether non-stationary cascade is indeed flexible enough to adjust itself to any current density required by the magnetosphere; (ii) being the simplest model it could be used as a testing ground for the numerical technique; (iii) boundary conditions in this model (no plasma inflow) are similar to that in the problem of electron–positron pair plasma generation near the horizon of a black hole (Beskin et al. 1992; Hirotani & Okamoto 1998), and, hence, from the solution of the pulsar problem it would be possible to get some hints to how to address the latter problem.

Ruderman & Sutherland (1975) estimate the height of the cascade zone for young pulsars (their equation 22) as

$$h_{\rm RS} \sim 5 \times 10^3 \rho_6^{2/7} P^{3/7} B_{12}^{-4/7} \,{\rm cm}\,, \tag{2}$$

where B_{12} is the pulsar magnetic field in units of 10^{12} G, ρ_6 is the radius of magnetic field line curvature normalized to 10^6 cm and P is the pulsar period in seconds. For young pulsars, with the period of the order of ~ 0.1 s, $h_{\rm RS}$ is less than the width of the polar cap

$$r_{\rm pc} \simeq 1.45 \times 10^4 P^{-1/2} \,{\rm cm}\,. \tag{3}$$

Therefore, 1D approximation should work well for such cascades. In the Ruderman–Sutherland model the charge density deviates strongly from the GJ charge density what creates accelerating electric field comparable to the vacuum electric field. The general relativistic effects introduce corrections to the electric field of the order of several per cent of the vacuum electric field (Beskin 1990; Muslimov & Tsygan 1990), and for this problem they can be ignored.

For young pulsars the dominant emission process in terms of the number of pair-production capable photons is the curvature radiation (e.g. Hibschman & Arons 2001a). In this paper, I am primarily interested in dynamics of the discharge zone, the region with the accelerating electric field. The size of that zone should be of the order of few $h_{\rm RS}$, which is of the order of the mean free-path of curvature photons. Synchrotron photons emitted by the injected pairs are much less energetic than curvature photons and, therefore, the mean-free path of synchrotron photons is much larger than $h_{\rm RS}$. They are absorbed at large distances from the NS where plasma density is expected to be very high and electric field is already screened. Hence, the pairs produced by the synchrotron photons do not influence the discharge dynamics, and synchrotron emission can be ignored.

So, the minimal physical model for the Ruderman–Sutherland cascade includes 1D electrodynamics, curvature radiation as the photon emission process and pair creation in a strong magnetic field as the source of electron–positron pairs.

3.2 Main equations

In the superstrong magnetic field of pulsar charged particles are in the first Landau level and move strictly along magnetic field lines. The radius of curvature of magnetic field lines ρ is much larger than the polar cap radius r_{pc}; for distances comparable to the width of the polar cap particle dynamics can be considered as a motion along straight lines. The curvature of the field lines is essential for photon emission and pair creation. The radius of curvature of magnetic field lines enters in the expressions for curvature radiation and gamma-ray absorption cross-sections as a parameter, which can depend on particle position.

I assume that charged particles move along straight magnetic field lines which are perpendicular to the NS surface. A coordinate axis x is directed along the field lines, its origin is at the NS surface and positive direction is towards the magnetosphere. In the 1D model charged particles are represented by thin sheath with infinite extend in the direction perpendicular to the x-axis. I normalize particle momentum to $m_e c$ – the normalized particle momentum p is its 4-velocity $p = \beta\gamma$, where $\beta = v/c$ is particle velocity normalized to the speed of light and $\gamma = (1 - \beta^2)^{-1/2}$ is the Lorentz factor. The equation of motion for a particle i is

$$\frac{dx_i}{dt} = v_i \qquad (4)$$

$$\frac{dp_i}{dt} = \frac{e}{m_e c}\frac{\tilde{q}_i}{\tilde{m}_i} E - W_{rr}, \qquad (5)$$

$\tilde{q}_i$ and $\tilde{m}_i$ are particle charge and mass in units of electron charge e and mass m_e correspondingly. W_{rr} is the term responsible for radiation reaction. For curvature radiation it is given by

$$W_{rr} = \frac{2e^2}{3 m_e c}\frac{\tilde{q}_i^2}{\tilde{m}_i}\frac{p^4}{\rho^2}. \qquad (6)$$

For low-energy particles radiation reaction becomes very small and for them W_{rr} in equation (5) is ignored (see Section 3.3).

In 1D model the only changing component of electromagnetic fields is the electric field component E parallel to the x-axis. The system is essentially electrostatic and the electric field can be obtained from the solution of the Poisson equation for the electric potential ϕ

$$\frac{d^2\phi}{dx^2} = -4\pi(\eta - \eta_{GJ}) \qquad (7)$$

as $E = -d\phi/dx$. Here η is the charge density and η_{GJ} is the GJ charge density. In order to solve equation (7) one has to either specify the potential difference across the domain or set the electric field to some fixed value at one end of the domain, either on the NS surface or at the base of the magnetosphere; these boundary conditions must be specified at every time-step. The main free parameter in the problem is the average current density which flows through the cascade zone. Charge can accumulate on the NS surface and particles can be sent back from the magnetosphere. Hence, boundary conditions are different at every time-step – the potential drop along the computation domain as well as the electric field at the domain boundaries change with time. Boundary conditions are related in some complicated way to the requirement of providing a certain value for the average current density. However, if charge conservation is taken into account, the electrostatic *boundary value* problem can be transformed into an *initial value* problem, which does not require boundary conditions. I do so in Appendix A, where

I derive the equation for the electric field[1]

$$\frac{dE(x, t)}{dt} = -4\pi(j(x, t) - j_m(t)). \qquad (8)$$

Here j is the current density at point x at time t, and j_m is the average current which flows through the calculation domain, determined by the twist of the magnetic field imposed by the global stress balance of the magnetosphere. To solve this equation only an initial configuration of the electric field in the domain $E(x)|_{t=0}$ is necessary; the boundary conditions are incorporated in j_m, i.e. the electric field at domain boundaries will adjust itself to provide the required average current density j_m.

The solution of equation (8) gives the correct electric field – the one which satisfies the Maxwell equations (in the 1D case it is the Gauss law) – if one starts from a configuration where E is obtained as a solution of the Poisson equation and numerical algorithm conserves electric charge. In my simulations, at the very first time-step I set some boundary conditions on the electric field (or the potential drop in the domain) and some initial particle distribution; then I compute the charge density η and solve the Poisson equation (7) for that boundary conditions to get the initial distribution of the electric field in the domain. At all subsequent time-steps for each point in the numerical grid I compute the electric field from its value at the previous time-step using equation (8); the current density j due to particle motion is calculated using a change conserving algorithm.

Physically, in order for electric field to be zero in the polar cap the charge density must be equal to the GJ charge density and the current density equal to the j_m required by the magnetosphere. The GJ charge density enters in the Poisson equation which is solved at the first time-step; because of charge conservation the system 'keeps memory' of the GJ charge density at all subsequent time-steps. The current density j_m enters in the equation for the electric field. So, the system tries to adjust to both these requirements.

Particles moving along curved magnetic field lines emit photons via the curvature radiation mechanism. Spectral energy distribution of curvature photons emitted by a particle with the Lorentz factor γ is given by the standard formula (Jackson 1975)

$$\frac{\partial N_{ph}}{\partial t\, \partial\epsilon}(\epsilon) = \frac{1}{\sqrt{3}\pi}\frac{\alpha_f c}{\lambda_C}\frac{1}{\gamma^2}\int_{\epsilon/\epsilon_{CR}^{peak}}^{\infty} d\xi\, K_{5/3}(\xi), \qquad (9)$$

where ϵ is the photon energy normalized to $m_e c^2$, α_f is the fine structure constant, $\lambda_C = \hbar/m_e c = 3.86 \times 10^{-11}$ cm is the reduced Compton wavelength, $K_{5/3}$ is the modified Bessel function of the order of 5/3; $\epsilon_{CR}^{peak} = (3/2)\lambda_C \rho^{-1}\gamma^3 \simeq 57.92\, \rho_6^{-1}\gamma_6^3$ is the peak energy of curvature photons, $\gamma_6 \equiv \gamma/10^6$. The integral in equation (9) has asymptotic forms

$$\int_y^{\infty} d\xi\, K_{5/3}(\xi) \simeq \begin{cases} 2.15 y^{-2/3} - 1.81, & \text{if } y \ll 1 \\ 1.25 e^{-y} y^{-1/2}, & \text{if } y \gg 1 \end{cases} \qquad (10)$$

The total number of curvature photons with energies greater than some ϵ_a emitted by the particle during time dt is

$$dN_{ph}(\epsilon > \epsilon_a) = dt\, \frac{1}{\sqrt{3}\pi}\frac{\alpha_f c}{\lambda_C}\frac{1}{\gamma^2} F\left(\frac{\epsilon}{\epsilon_a}\right) \qquad (11)$$

where

$$F(\zeta) = \int_\zeta^{\infty} d\xi \int_\xi^{\infty} dx\, K_{5/3}(x). \qquad (12)$$

---

[1] Levinson et al. (2005) used the same approach for the calculation of the electric field. They did not elaborate on the physical meaning of j_m, so I decided to present a detailed derivation of equation (8).

For small values of its argument $F(\zeta)$ has the following asymptotic form:

$$F(\zeta) \simeq 1 + 0.346\zeta - \zeta^{1/3}(1.232 + 0.033\zeta^2), \quad \zeta \ll 1. \quad (13)$$

Only very high-energy photons capable of producing an electron–positron pair in the calculation domain are of relevance for the considered problem and only those are tracked in the code (see Section 3.3).

I assume that photons are emitted tangentially to the magnetic field lines and then move along straight lines. The angle ψ between the photon momentum and the magnetic field increases as the photon propagates further from the emission point. In a simple model where magnetic field lines have constant curvature the angle between the photon momentum and the magnetic field is given by

$$\psi(x) = (x - x_e)/\rho, \quad (14)$$

where x_e is the coordinate of the emission point. In the dipolar magnetic field the expression for $\psi(x)$ is slightly more complicated

$$\psi(x) \simeq \frac{3}{4}\theta_e \frac{x - x_e}{x} \sqrt{1 + \frac{x_e}{R_{NS}}}, \quad (15)$$

here θ_e is the colatitude of the emission point (a free parameter in the 1D model) and R_{NS} is the NS radius. Both models were used in the simulations. The cross-section of photon absorption is given by (Erber 1966)

$$\sigma_{B\gamma} = 0.23 \frac{\alpha_f}{\lambda_C} \frac{B}{B_q} \sin\psi \, \exp\left(-\frac{8}{3\chi}\right), \quad (16)$$

where $\chi = \epsilon B \sin\psi / B_q \simeq 2.27 \times 10^{-2} \epsilon B_{12} \psi$, and $B_q = m_e^2 c^3 / e\hbar \simeq 4.41 \times 10^{13}$ G is the critical magnetic field strength. The cross-section grows exponentially as photon propagates further from the emission point.

When the photon is absorbed I assume that its energy is equally divided between newly created electron and positron. The perpendicular component of particle's momentum will be rapidly radiated as synchrotron photons, which, as described before, are neglected. Injected particle ends up having only the longitudinal component of the momentum

$$p_{e^\pm} \simeq \left(\frac{\epsilon^2 - 4}{4 + \psi_a^2 \epsilon^2}\right)^{1/2}, \quad (17)$$

where ψ_a is the angle between the photon momentum and the magnetic field at the absorption point.

3.3 Numerical implementation

In this section I describe normalization of physical quantities, introduce several numerical parameters controlling the algorithms and give their typical values in my simulations. I also give an overview of main numerical algorithms used in the code; a detailed description of the numerical code will be given elsewhere.

Distances are normalized to the radius of the pulsar polar cap, $x_0 = r_{pc}$, given by equation (3). The electric potential is normalized to the vacuum potential drop between the rotation axis and the edge of the polar cap in the aligned rotator

$$\Phi_0 = \frac{\Omega}{c} \frac{Br_{pc}^2}{2} \simeq 6.6 \times 10^{12} B_{12} P^{-2} \text{ V}, \quad (18)$$

where Ω is the pulsar angular velocity. The electric field is normalized to

$$E_0 = \frac{\Phi_0}{x_0} \simeq 4.6 \times 10^8 B_{12} P^{-3/2} \text{ V cm}^{-1}, \quad (19)$$

and the charge density to the absolute value of the GJ charge density

$$\eta_0 \equiv \frac{\Omega B}{2\pi c} = \frac{\Phi_0}{\pi x_0^2}. \quad (20)$$

Each numerical particle is a macroparticle representing a (large) number of real particles N_0, either electrons or positrons. Each numerical particle has a statistical weight $w_i = \tilde{w}_i N_0$. When a macroparticle emits a photon, the latter gets the particle's statistical weight (also see below the description of photon sampling); when the photon is absorbed the injected electron and positron get the photon's statistical weight. An important numerical parameter is N_{GJ}^{cell} – the number of macroparticles with the normalized statistical weight $\tilde{w}_i = 1$ in a cell which create the GJ charge density

$$\eta_0 = eN_0 N_{GJ}^{cell}. \quad (21)$$

The parameter controlling the number of numerical particles in the simulation is N_{GJ}^{cell}; N_0 is computed at the start of the simulation from equation (21). The difference in the number density between particles of opposite signs of the order of N_{GJ}^{cell} results in a large electric field; this number should be not very small, otherwise numerical noise will strongly contaminate results. In my simulations values of $N_{GJ}^{cell} \gtrsim 5$ provide acceptable level of numerical noise which allows to recognize plasma oscillation excited in the pair plasma.

The calculation domain is divided in M_x equal numerical cells; a typical value of M_x in my simulations is several thousands. I use 1D version of the charge conservative algorithm proposed by Villasenor & Buneman (1992) for scattering of charge and current densities to the grid points and for interpolation of the electric field to particle locations. Integration in time of equations (4), (5), (8) is done with a leap-frog scheme with a uniform time-step Δt. The radiation reaction in equation (5) is taken into account only for particles with momentum larger than a certain value p_{rr}^{min}.

For each particle if its momentum is larger than a certain value p_{rad}^{min} I calculate the mean number of photons N_{ph} with energies larger than a certain ϵ_{em}^{min} the particle emits during time Δt according to equation (11). If N_{ph} is small, less than a certain N_{ph}^{max}, I sample the number of actually emitted photons from the uniform distribution with the mean value equal to N_{ph}. Then for each photon I sample its energy from the distribution given by equation (12) using either cutpoint or inverse transform methods (Fishman 1996). The values of $F(\zeta)$ in equation (12) are tabulated for $0.01 \leq \zeta \leq 10$ for use in the cutpoint method; for smaller ζ inverse transform method is used with the asymptotic formula $F(\zeta) \simeq 1 - 1.232\zeta^{1/3}$. If $N_{ph} > N_{ph}^{max}$, the particle emits a fixed number of numerical photons – the spectrum is divided in N_{CR}^{bin} bins, the number of emitted numerical photons is equal to N_{CR}^{bin}; each photon gets a statistical weight equal to the product of the statistical weight of the emitting particle and the number of photons emitted in the corresponding spectral energy bin given by equation (9).

To calculate the position where the photon is absorbed I sample the optical depth the photon should achieve before being absorbed; then I integrate the cross-section (16) along photon's trajectory until the required optical depth is reached. The cross-section of photon absorption in the polar cap grows exponentially with the distance from the emission point, and most of the trajectory do not make significant contribution to the optical depth. At first optical depth along photon's trajectory is calculated using rectangle methods with large spatial steps ($\sim 1/20$–$1/40$ of the domain size) until the optical depth on the next step would exceed the required value. This integration method overestimates the optical depth; the trajectory always continues beyond this intermediate stop point. I redo the cross-section integration between the emission and the stop points

using 15 points Gauss–Kronrod integrator that provides a very accurate value for the optical depth at the stop point. Then, the optical depth integration is proceeded with a smaller spatial step comparable to the cell size. The number of cross-section evaluation in this algorithm is, on average, by a factor of few tens smaller than a cross-section integration with the step equal to the cell size would require.

Values of the numerical parameters p_{rr}^{min}, p_{rad}^{min}, ϵ_{em}^{min}, N_{ph}^{max}, N_{CR}^{bin} are fixed at the start of the simulation. These values are chosen to sample all pair creation capable photons and correctly account for the radiation reaction on one side, and to minimize the computation time of the other side; their particular values depend on physical conditions: the pulsar period, the magnetic field strength and the radius of curvature of magnetic field lines. The typical values I used in the simulations: $p_{rr}^{min} \sim p_{rad}^{min} \sim 10^5 - 10^6$, $\epsilon_{em}^{min} \sim 2-40$, $N_{ph}^{max} \sim N_{CR}^{bin} \sim 50$.

The numerical code was developed from scratch and written in C++ programming language. Its modular object-oriented structure is designed to facilitate further extension to multi-dimension and incorporation of additional physical processes. I tested the PIC part of the code performing simulations of the following test problems: oscillation of two test particles, two stream instability in both relativistic and non-relativistic regime, non-relativistic and relativistic Child's laws, dependence of plasma frequency on numerical resolution (Birdsall & Langdon 1985). I also tested that the code is indeed change conservative up to machine precision. The Monte Carlo part of the code was tested as follows. I verified that the energy distribution of emitted photons agrees with the spectrum of curvature radiation. For several fixed emission points, different values of photon energy, magnetic field strength and radius of curvature of magnetic field lines I compared the distribution of photon absorption points produced by the Monte Carlo code with the corresponding theoretical distributions. I also checked that for a given time interval the total energy of emitted photons is equal to the particle radiation-reaction losses.

4 RESULTS OF NUMERICAL MODELLING

The numerical simulations have shown that in the Ruderman–Sutherland model pair creation is quasi-periodic and self-sustained. I performed simulations for different initial particle distributions, initial electric fields, strengths of the magnetic field, radii of curvature of magnetic field lines and pulsar periods. Independent of the initial configuration for non-zero j_m pair-creation process begins some time after the start of simulations. How and how much plasma is formed in this initial burst depend on the specific setup. The plasma generation stops after enough plasma is produced to screen the electric field. After plasma generated in this burst of pair formation leaves the domain (in a couple of domain flyby times), the behaviour of the cascade for given magnetic field, pulsar period and the mean current j_m is the same, independent of the initial configuration. All subsequent bursts of pair formation do not depend on the initial setup – the system seems to forget the initial conditions. After that initial burst of pair creation the cascade zone always settles down to a quasi-periodic behaviour. For a given j_m cascade behaviour is qualitatively similar for all other physical parameters admitting pair creation.

I describe here main properties of the Ruderman–Sutherland cascade using as an example a pulsar with period $P = 0.2$ s, magnetic field $B = 10^{12}$ G and the radius of curvature of magnetic field lines $\rho = 10^6$ cm. The radius of curvature of magnetic field lines comparable to the NS radius implies that there is a non-dipolar component of the magnetic field in the polar cap region. I performed simulations for pure dipole magnetic field with $\rho \sim 10^8$ cm too. Qualitatively results do not depend on the radius of curvature, but for smaller ρ calculations with the same numerical resolution can be done faster because the size of the gap with accelerating electric field is smaller. On the other hand, the adoption of this value for ρ simplifies comparison with the original Ruderman & Sutherland (1975) model, where the same value for ρ was used.

The polar cap radius for such pulsar is $r_{pc} = 3.24 \times 10^4$ cm (equation 3). The heights of the gap should be (see equation 2)

$$h_{RS,1} \simeq 2.5 \times 10^3 \text{ cm} \simeq 0.077 r_{pc}, \qquad (22)$$

and the potential drop in the gap is

$$\Delta V_{RS,1} = 2\pi\eta_{GJ} h_{RS,1}^2 \simeq 1.98 \times 10^{12} \text{ V} = 0.012\Phi_0, \qquad (23)$$

so the maximum Lorentz factor of electrons and positrons is

$$\gamma_{RS,1}^{max} = \frac{e\Delta V_{RS,1}}{m_e c^2} \simeq 3.87 \times 10^6. \qquad (24)$$

The angular velocity of NS rotation is anti-parallel to the magnetic moment of the star and the GJ change density is positive. The length of the computation domain for the simulations described in this section is $L = 0.3 r_{pc} \simeq 9.72 \times 10^3$ cm. Numerical grid has $M_x = 5000$ points, so that the cell size is $\Delta x \simeq 1.94$ cm. The number of numerical particles in cell providing the GJ charge density $N_{GJ}^{cell} = 10$. Other numerical parameters are $p_{rr}^{min} = p_{rad}^{min} = 5 \times 10^5$, $\epsilon_{em}^{min} = 20$, $N_{ph}^{max} = 50$, $N_{CR}^{bin} = 80$.

I describe properties of cascade with physical parameters given above for three different current densities: $j_m = j_{GJ}$, $j_m = 0.5 j_{GJ}$ and $j_m = 1.5 j_{GJ}$. First I describe the main properties of cascade with $j_m = j_{GJ}$. Pair formation dynamics for different current densities is qualitatively similar. Later in this section I will highlight the differences in cascade properties for $j_m = 0.5 j_{GJ}$ and $j_m = 1.5 j_{GJ}$.

4.1 Pattern of plasma flow

In this subsection, I describe the pattern of plasma flow for a typical cycle of pair formation in cascade with $j_m = j_{GJ}$. Cascade development is illustrated by a series of snapshots at several time moments during a cycle of pair formation taken from a long simulation where several such cycles were observed.[2] In Fig. 2, I plot the change density at equally spaced time interval during the discharge cycle. In the upper panel of that figure, I present an overview of the entire cycle, in the lower panel I plot snapshots of the change density distribution at smaller time intervals for the most interesting part of the discharge – formation of a new plasma blob. In Figs 3 and 4, more detailed information about physical conditions in the discharge zone is shown: the number densities of electrons and positrons $\eta_\pm$, the accelerating electric field E, phase portraits ($p - x$ diagrams) of electrons, positrons and pair producing photons. In the phase portraits particles with positive values of four-momentum p are those which move from the NS, particles with negative p move towards the NS. The time t in these figures is normalized to the flyby time of the computational domain – the time a relativistic particle needs to cross the domain L/c. The time is counted from the start of a particular simulation, so its absolute value has no physical

---

[2] In a previous short publication (Timokhin 2009) I presented plots similar to Figs 2 and 4 of this paper for a different cycle of the same simulation. Comparing these plots one can see that different bursts of pair formation are indeed very similar.
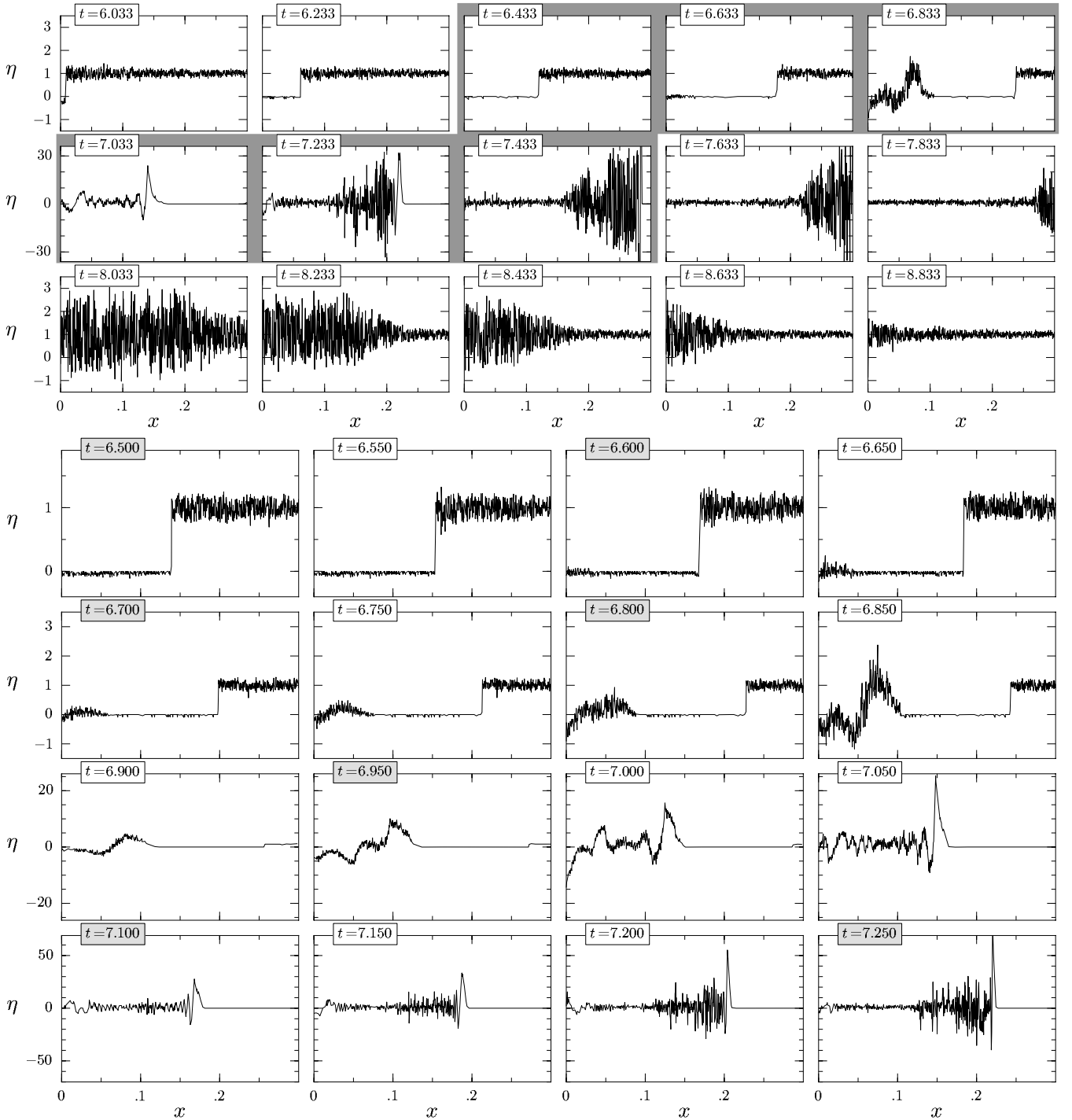
Figure 2. Snapshots of charge density distribution in the calculation domain for cascade with $j_{\mathrm{m}} = j_{\mathrm{GJ}}$. Charge density η as a function of distance x from the NS is plotted at equally separated moments of time; η is normalized to the GJ change density η_{GJ}. The time t shown in small square boxes is normalized to the flyby time of the computation domain and is counted from the start of the simulation. The presented cycle is taken from the middle of a long simulation. Top: the *whole* cycle of cascade development. Bottom: snapshots for time interval marked by the grey area in the top panel; these snapshots illustrate formation and propagation of plasma blob in more detail.

meaning – only time intervals between the shots have physical meaning.

Each pair creation cycle could be conveniently divided into three phases: (i) vacuum gap formation (timeshots for $t = 6.033$–6.633 in Fig. 2), (ii) formation and propagation of a plasma blob ($t = 6.633$–7.833) and (iii) relaxation ($t = 7.833$–8.833). Each burst of pair

formation generates dense electron–positron plasma which screens the electric field. Particles must leave the domain in order to provide the required current density. When plasma leaves the polar cap a gap with almost no particles inside is formed; the vacuum electric field in the gap is no longer screened [phase (i)]. The few particles in the gap are accelerated and emit high-energy gamma-photons, and
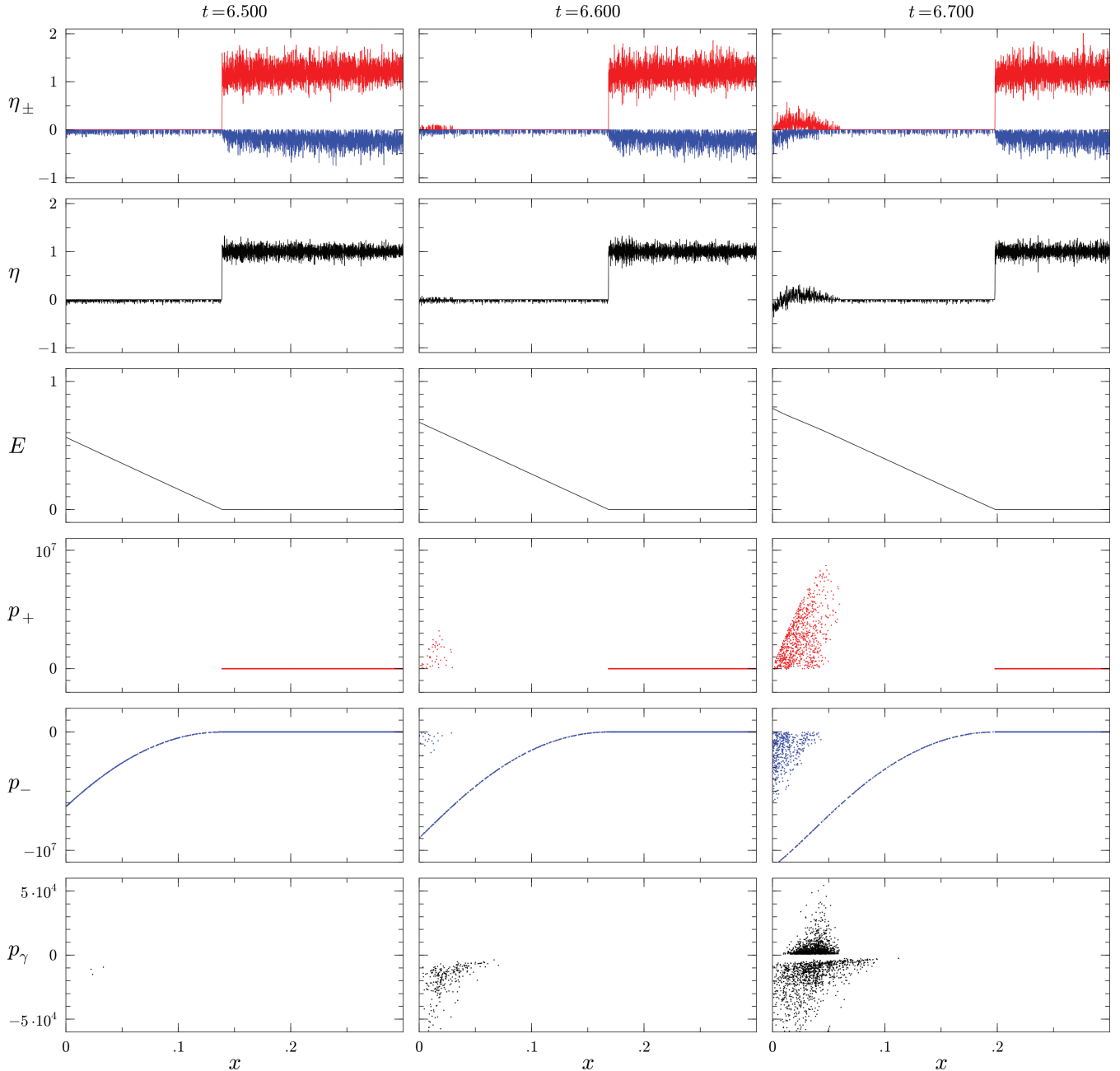
Figure 3. Ignition of pair formation in cascade with $j_m = j_{GJ}$. Several physical quantities are shown as functions of the distance x from the NS. Plots in each column (for the same time t) are aligned – they share the same values of x. Snapshots are take at time moments of the first three marked snapshots in the bottom panel of Fig. 2. The following quantities are plotted: first row: $\eta_\pm$ – charge density of electrons (negative values, blue line) and positrons (positive values, red line); $\eta_\pm$ is normalized to the GJ charge density η_{GJ}. Second row: the total charge density η normalized to the GJ charge density η_{GJ}. Third row: accelerating electric field E normalized to the vacuum electric field E_0. Fourth row: phase-space portrait of positrons (horizontal axis – positron position x, vertical axis – positron momentum p_+ normalized to $m_e c$). Fifth row: phase-space portrait of electrons (horizontal axis – electron position x, vertical axis – electron momentum p_- normalized to $m_e c$). Sixth row: phase-space portrait of pair-producing photons (horizontal axis – photon position x, vertical axis – photon momentum p_γ normalized to $m_e c$).

the process of plasma creation starts again. The electron–positron plasma is produced non-uniformly; it forms a blob[3] of relativistic plasma where large amplitude plasma oscillations are excited [phase (ii)]; the blob is visible in Fig. 2 as a packet of large amplitude charge

density oscillations. The blob moves into the magnetosphere leaving a tail of moderately relativistic plasma behind. When the blob leaves the computational domain, the remaining plasma still screens the vacuum electric field till the plasma density drops below n_{GJ} and pair formation starts again [phase (iii)]. Below I describe these processes in more details.

A typical cycle starts with the formation of a vacuum gap above the NS surface (timeshots at $t = 6.033$–6.650 in Figs 2 and 3). The

---

[3] Actually, I am computing plasma sheets in 1D, but in 2D and 3D these would be plasma 'blobs', so I use the latter term throughout the paper.
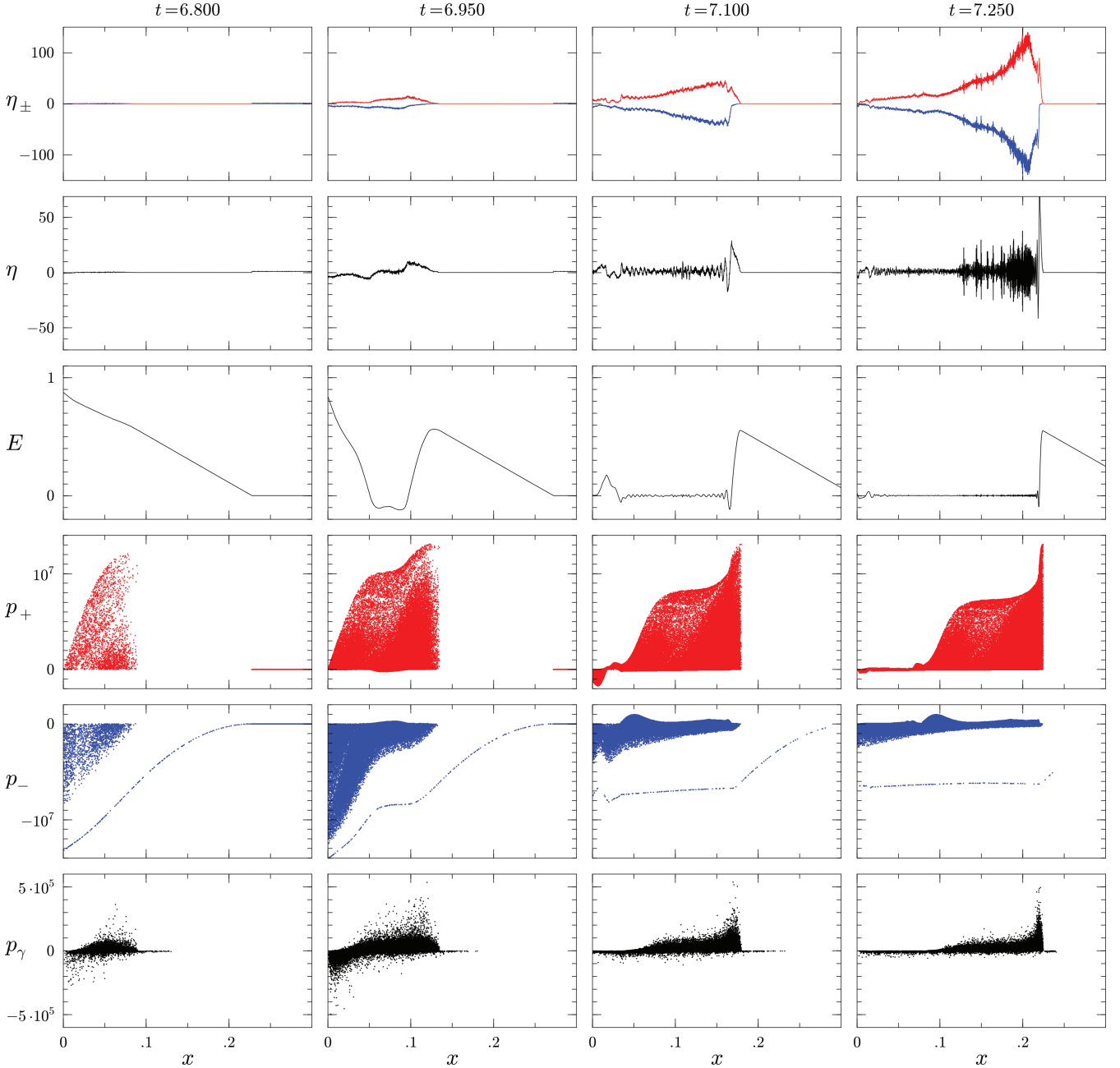
Figure 4. Screening of the electric field in cascade with $j_m = j_{GJ}$. Snapshots are take at time moments of the last four marked snapshots in the bottom panel of Fig. 2. The same quantities are plotted as in Fig. 3.

gap forms because plasma leaves the domain in order to provide the required current density j_m. The GJ charge density is positive, and when the electric field is completely screened there are more positrons than electrons. The current density is positive, and positrons, on average, must flow towards the magnetosphere (to the right). As there is no plasma inflow through the domain boundaries, the gap forms when there are not enough charged particles to provide the required current and change densities in the whole domain; above the gap the plasma still sustains the required current and change densities. Positrons flow into the magnetosphere, so the gap forms at the NS surface.

Pair creation starts close to the NS and is ignited by gamma-rays emitted by electrons flowing *towards* the NS. These primary

electrons have been created in the previous burst of pair formation; they leak from the tail of the plasma blob formed in the previous cycle and enters the gap from above. These electrons are visible as a thin line of particles with negative momenta p_- in the electron phase-space portraits (the fifth row in Fig. 3). Pair-production capable gamma-photons emitted by these electrons have negative momenta and are visible in the photon $p - x$ diagrams as scattered dots with negative p_γ at $t = 6.5$, 6.6. These photons are eventually absorbed and create electron–positron pairs, which are visible as scattered dots at the left in the electron and positron $p - x$ diagrams at $t = 6.6$–6.7. These newly created electrons and positrons are accelerated by the strong electric field of the gap (see timeshot at $t = 6.6$); when they have been accelerated up to Lorentz factors of the order of several

10^6 they start to emit pair-production capable photons. At $t = 6.700$ there are already gamma-photons with positive momenta; they have been emitted by the secondary positrons accelerated in the strong vacuum electric field. At these early stages of pair discharge the density of the newly created plasma is still very low (see plots for $\eta_\pm$, the first row in Fig. 3), and the electric field is not influenced by the injected plasma (the third row in Fig. 3). All electrons and positrons are accelerated up to high Lorentz factors and start emitting pair-production capable gamma-photons very soon.

The secondary electrons and positrons are accelerated in opposite directions, and plasma start being polarized (see distribution of the charge density at $t = 6.8, 6.85, 6.9$ in Fig. 2). The polarization of plasma creates an electric field opposite to the vacuum field, and the effective accelerating electric field decreases. When the particle number density becomes comparable to the GJ density n_{GJ} the accelerating electric field starts being screened by plasma. How the electric field is screened is shown as a series of snapshots in Fig. 4. The screening naturally starts in the place where plasma density is maximal. When more and more plasma is injected the region of screened electric field broadens till it eventually extends up to the NS surface.

The particles which produce most of the pair creating photons are the secondary positrons which have been accelerated at the time when plasma density was small and electric field was strong. Secondary electrons have been accelerated up to very high energies too, but they have been moving towards the NS – they slammed into the NS surface and do not contribute to pair creation at later times. The high-energy positrons move into the magnetosphere emitting gamma-rays which turn into electron–positron pairs. These positrons practically comove with the gamma-rays. Freshly created pairs are relativistic and have momenta directed from the NS; most of them will remain relativistic and will move into the magnetosphere. So, the pair plasma forms a blob with constantly increasing particle density (see the first row in Fig. 4).

Photons cannot go ahead of relativistic particles at the front edge of the blob, and pairs are injected only inside the blob. As the plasma blob moves into the magnetosphere so does the vacuum gap limited from below by the front edge of the blob. Ahead of the blob there is practically vacuum with strong electric field, as there are only electrons leaking from the tail of the previous blob and their number density is very low. The electric field inside the blob is screened by the plasma. At the front of the blob a sheath of positive charge is formed which screens the vacuum electric field. This sheath is visible as a large spike in the charge density distribution at timeshots $t = 7.05$–7.433. Inside the sheath the electric field goes from the vacuum value to its very low value in the blob. Pairs injected in this sheath by conversion of gamma-photons emitted by the particles which are already in the sheath are accelerated by that electric field and start emitting gamma-rays too. As more and more pairs are ejected there the width of the sheath decreases. However, the number of particles in the sheath is small (see the plot for $\eta_\pm$ in Fig. 4 at $t = 7.25$). Pairs injected in other parts of the blob are not accelerated because the electric field there is screened. Hence, subsequent pair formation is driven mostly by particles accelerated at early stages of the discharge, when the electric field was strong. As these particles are emitting gamma-rays and they are not accelerated anymore, their kinetic energy decreases. This can be seen in the positron $p - x$ diagrams in Fig. 4; the spike of high-energy particles at the blob's front is due to particle acceleration in the charge sheath.

I observe thermalization of freshly created electrons and positrons in the simulations. Low-energy particles are present starting from very early stages of blob formation. Some of the low-energy par-

ticles are reversed back. While the bulk of the plasma moves with relativistic speed into the magnetosphere some particles are left behind forming a 'tail' of the blob which has much lower particle number density than the blob itself. Although the fraction of particles left behind is small, their number is enough to screen the vacuum electric field for some time, preventing immediate formation of a new vacuum gap after the blob detaches from the NS.

While the general structure of the flow is evident from the performed simulations, some questions remain unanswered. The most important among them is about the time between discharges. It depends on the rate of plasma leakage from the blob – the more particles leak out, the later the next gap forms. Due to continuous pair injection plasma density in the blow increases enormously and at some time the numerical scheme stops resolving the Debye length of the plasma, and results start depending on the numerical resolution. Because of this the blob cannot be followed for time interval long enough (and distances large enough) to get the repetition rate of the cascade. In the presented simulations the size of the simulation zone is set such that the blob leaves calculation domain before the numerical scheme fails to model it correctly. When the blob leaves the calculation domain particles are still leaking from it into the tail. When the blob is no longer in the computational domain, particle supply to the tail is stopped and the time interval during which plasma density in the domain drops to the GJ density – and a new gap begins to form – is substantially smaller in my simulations than it would be in reality. Duration of the relaxation phase in the simulations (timeshots $t = 7.833$–8.833) is strongly influenced by the numerical setup.

However, I believe that the qualitative behaviour of the plasma during this phase is represented correctly, as there are no physical processes in the blob tail except the particle supply from the blob that the code fails to model when the blob is no longer in the computational domain. There is no particle acceleration in the tail and pair creation is only due to electrons which leak from the previous blob and are accelerated towards the NS in the travelling vacuum gap. The number of these electrons is negligible compared to the number of pair-producing positrons in the blob. The fraction of particles leaking from the blob when it is still inside the domain is also small, of the order of a few per cent. This is enough to screen the vacuum electric field, but the energy carried by those particles is negligible compared to the energy carried by particles in the blob (see Section 4.4). Hence, the only cascade characteristic substantially influenced by the rate at which particles leak from the blob is the repetition rate of pair creation bursts. Already from these simulations, it is clear that the time between discharges is longer than the vacuum gap crossing time h_{RS}/c. This introduces a new time-scale into the Ruderman–Sutherland model.

Qualitatively the plasma flow after the discharge should be as follows. The tail consists of particles leaked from the blob; those are mildly relativistic particles, some of them are trapped in plasma oscillations and, on average, the tail moves with a subrelativistic velocity. The vacuum gap is limited from above by the tail of the previous blob: the plasma must move in order to support the current density j_m; when the plasma density drops to values comparable to the GJ density, the plasma cannot support the required current density and the GJ charge density at the same time, a gap appears, and so the tail ends in a vacuum gap. Among the trapped particles in the tail there are both electrons and positrons which move towards the NS. The electrons at the tail's end enter the gap and get accelerated towards the NS – they will be the primary particles in the next burst of pair formation. The positrons entering the gap are reversed and are sent into the magnetosphere. The upper boundary of the

vacuum gap – the tail's end – moves with a subrelativistic veloc-ity, the front of the blob is formed by ultra-relativistic positrons and moves relativistically; therefore, the gap shrinks when the blob moves into the magnetosphere. The velocity of the blob's tail v_{tail} is several per cent less than the speed of light, $v_{\text{tail}} \sim 0.95$–$0.99\,c$. Eventually the front of the new blob catches the tail of the previous blob; the disappearance of the gap is directly visible in the case of $j_{\text{m}} = 0.5 j_{\text{GJ}}$ (see Section 4.5). Therefore, the magnetosphere in the open field line zone will be filled with plasma everywhere and starting at some distance from the polar cap there will be no gaps in plasma spacial distribution.

4.2 Superluminal plasma wave

When plasma starts being injected into a region with strong electric field it is polarized and starts screening the electric field. During the process of screening of the vacuum electric field large-amplitude oscillations are excited in the injected pair plasma; these oscillations are visible in timeshots starting at $t = 6.85$ and until the blob leaves

the domain. Screening of the electric field starts in the middle of the blob and spreads to its edges. This spreading occurs in the form of an electrostatic wave. The propagation of the wave can be seen in Fig. 5 where I plot snapshots for the electric field, the charge density and the particle number density for the same spatial domain where the blob is being formed for 6 moments of time; I plot also three vertical lines which mark fiducial positions moving with the speed of light towards the magnetosphere. One can clearly see that the phase velocity of the wave is greater than the speed of light; also note that the wave propagating towards the NS is superluminal too. In the process of electric field screening less and less charge separation would be necessary to kill the electric field. Apparently this is the reason why the wavelength of plasma oscillations decreases. At the time of wave formation the particle number density is already very high; there are more than ~ 100 numerical particles per cell. The Debye length of the plasma – calculated as

$$\lambda_{\text{D}} \sim \frac{c}{\omega_p} = c \left(\frac{4\pi e^2}{m_{\text{e}}} \int \frac{n(\gamma)}{\gamma^3} \, \mathrm{d}\gamma \right)^{-1/2}, \qquad (25)$$
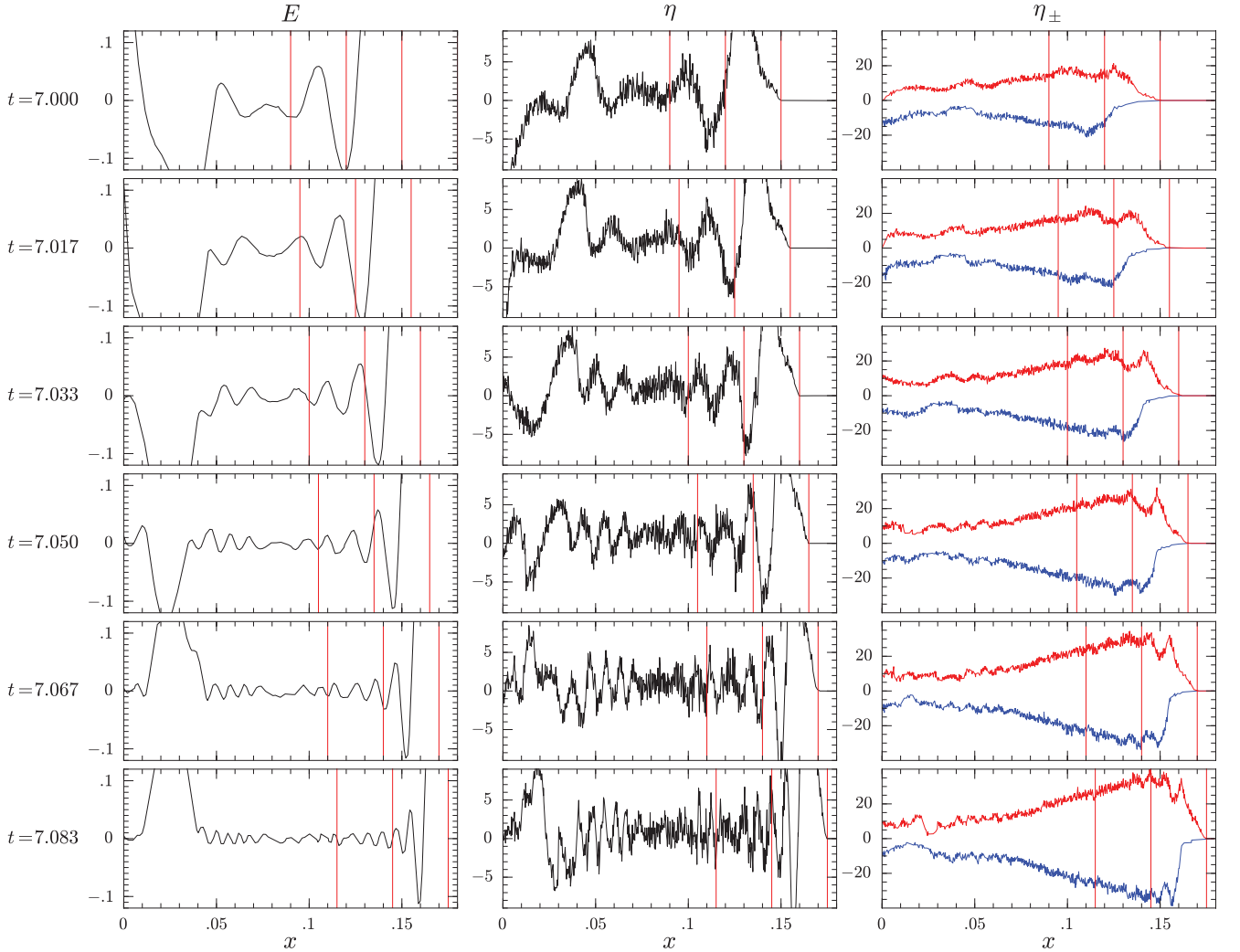

Figure 5. Formation and propagation of superluminal electrostatic wave in the forming plasma blob for cascade with $j_{\text{m}} = j_{\text{GJ}}$. There are six snapshots for the electric field E, the total change density η and the charge density of electrons (negative values, blue line) and positrons (positive values, red line) $\eta_{\pm}$. All quantities are plotted as functions of distance x for the part of the calculation domain where the blob is forming. Snapshots are taken at equally separated time intervals. Plots in each column are aligned and share the same values of x. The same normalizations for physical quantities are used as in Fig. 3. The three thin red vertical lines in each plot mark fiducial points moving with the speed of light towards the magnetosphere. The wave is superluminal; its maxima move faster than these lines.
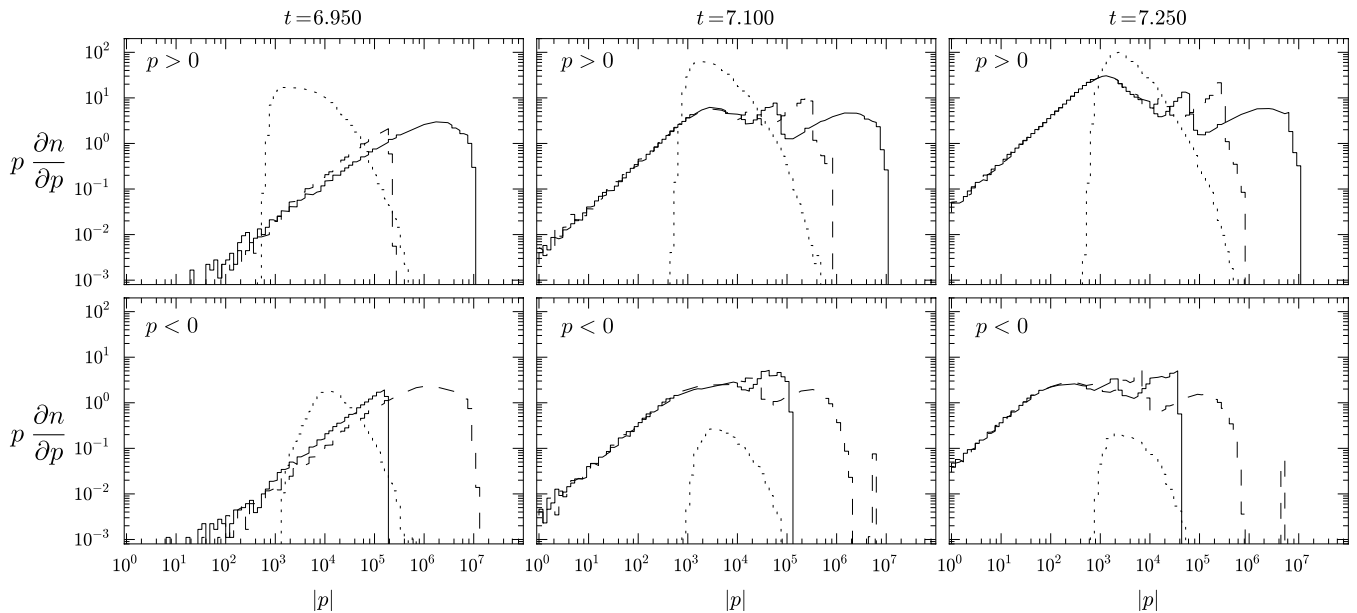
Figure 6. Particle momentum distribution for plasma in the blob at three moments of time for cascade with $j_m = j_{GJ}$. Positron distributions are shown by solid lines, electron distributions by dashed lines and the distribution of pair producing photons by dotted lines. Plots in the top row show distributions for particles moving towards the magnetosphere ($p > 0$), and plots in the bottom row show distributions for particles moving towards the NS ($p < 0$). Each column corresponds to the same moment of time shown above the plots. Plots in each columns are aligned and share the same values of $|p|$. The following blob sizes were assumed: $x \in [0, 0.135]$ for $t = 6.95$, $x \in [0.05, 0.18]$ for $t = 7.1$ and $x \in [0.1, 0.225]$ for $t = 7.25$.

where $n(\gamma)$ is the number density of particles with the Lorentz factor γ – is resolved; at the time the snapshots shown in Fig. 5 are made λ_D is several tens of times larger than the cell size. Hence, these oscillations are not numerical artefacts. The electric field in the wave is too weak to accelerate particles up to energies when they can emit pair-production capable photons. Particle injection rate is set by very high-energy particles accelerated at earlier time and there is no back reaction of the wave on the particle production rate.

Decreasing of the wavelength eventually ends when the wavelength becomes equal to the cell size. From that moment the code cannot correctly follow propagation of the wave. In timeshots for $t > 7.25$ the wavelength is not resolved anymore. Oscillations persist, but because the wavelength is equal to the cell size, parameters of the wave depend on the numerical resolution and so tell us little about how the wave would propagate at that time in a real cascade. However, based on the information obtained at the early stages of wave evolution (for $t < 7.25$) – when results of numerical modelling should be reliable – I would like to make the following remarks. Being superluminal this wave is not damped via Landau damping. I may speculate that this wave could stay superluminal, with its phase speed approaching the speed of light from above, for a time long enough that it can travel into the magnetosphere practically undamped. Although in my 1D simulations the wave is electrostatic, in reality it would be electromagnetic. It could escape the magnetosphere and be observed as coherent pulsar emission, or/and it can excite another electromagnetic wave(s) which escape the magnetosphere.

4.3 Particle momentum redistribution and current adjustment

Starting from very early stages of blob formation the injected pairs start being thermalized. I use the term 'thermalization' here rather

loosely, meaning that in the particle momentum distribution there is a strong broad component which peaks at some momentum value; it extends up to very low energies decreasing like a power law, and decreases strongly after the peak. Although I did not perform a formal fitting procedure for particle momentum distribution,[4] the low-energy tail of the 'thermal' component follows the 1D Maxwell–Juttner distribution $\partial n / \partial p \sim$ const for small p quite good. In Fig. 6, I plot particle momentum distribution $p (\partial n / \partial p)$ for three different moments of time. In the upper panel I plot the momentum distribution of particles moving towards the magnetosphere, p is positive; in the lower panel – the momentum distribution of particles moving towards the NS, p is negative. These distributions are for particles in the blob – they are averages over $x \in [0, 0.135]$ for $t = 6.95$, $x \in [0.05, 0.18]$ for $t = 7.1$ and $x \in [0.1, 0.225]$ for $t = 7.25$ (cf. plots for the particle number density in Fig. 4). There are low-energy particles and there are particles with both direction of motion in the blob. Essentially the pair plasma becomes four-component: (i) positrons moving into the magnetosphere, (ii) positrons moving toward the NS, (ii) electrons moving into the magnetosphere, (iv) electrons moving towards the NS. Such four-component plasma easily adjusts locally to both requirements of providing the GJ charge density and the current density j_m.

At initial phases of blob formation at least one of the processes leading to plasma thermalization is trapping of particles in the electric field of the plasma wave. In Fig. 7 trajectories for three of such trapped pairs are shown. In that figure, phase trajectories of pair-producing photons are plotted by dotted lines, marked as $\gamma_{1,2,3}$.

---

[4] To get an accurate momentum distribution, it is necessary to collect enough numerical particles. This leads to averaging over a macroscopic volume with different physical conditions, and results of such fitting would be ambiguous anyway.
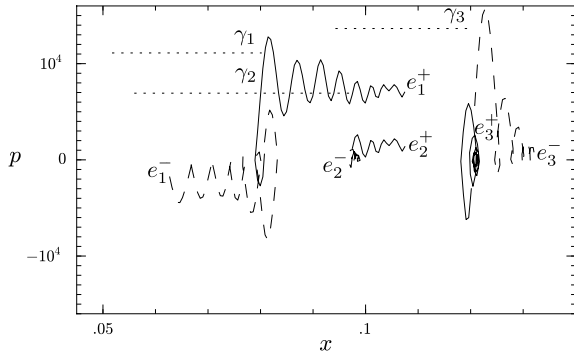
Figure 7. Trajectories of three pairs and their parent photons in the phase space (distance x is along the horizontal axis, momentum p is along the vertical axis) for cascade with $j_\mathrm{m} = j_\mathrm{GJ}$. Trajectories of pair creating photons are shown by dotted lines and marked as $\gamma_{1,2,3}$. Trajectories of positrons are shown by solid lines and marked as $e^+_{1,2,3}$, trajectories of electrons are shown by dashed lines and marked as $e^-_{1,2,3}$. Marks are located at the ends of corresponding particle trajectories. All trajectories end at $t = 7.1$.

When photon is absorbed an electron and a positron are injected.[5] Electron trajectories are shown by dashed lines, positron trajectories by the solid lines; trajectories' final points are marked as $e^-_{1,2,3}$ and $e^+_{1,2,3}$ correspondingly. Particle trajectories end at $t = 7.1$; at that and earlier time both the Debye length and the wavelength of the wave are well resolved. They are tens of times larger than the cell size, and there are many particles per cell; particle trajectories are well resolved too. Hence, the thermalization is not a numerical artefact. Thermalization of freshly injected pairs proceeds also at later stages of cascade development; however, as the code does not resolve the plasma wave anymore, it is not possible to disentangle the influence of the wave on the thermalization process at this time.

From the current simulations, it is not clear what is the fate of the plasma wave in the blob. If it exists for a long time, particle thermalization in these oscillations could continue. On the other hand, deviation of the current density from j_m results in the appearance of an electric field even if the charge density is equal to the local GJ charge density. The presence of that electric field in a plasma with broad momentum distribution might result in some instability which could facilitate pair thermalization – at least I see plasma thermalization during the relaxation phase when there is no large amplitude plasma wave and plasma leaves the domain adjusting to the required current density by redistribution of particle momenta. This topic, however, needs additional investigation and will be addressed in future publications.

To reverse the direction of motion of low-energy particles a weak electric field would be sufficient. For charge density to be equal to the local GJ charge density the number of positrons should be greater than the number of electrons by n_GJ. In order to provide current density less than j_GJ some positrons should move towards the NS. If there is a population of low-energy trapped positrons, a weak fluctuating field can ensure that some trapped positrons *on average* will be moving towards the NS. A similar process can provide a current density larger than j_GJ and still keep the change density equal to the GJ charge density. The adjustment of the current density can proceed in the cascade zone *locally*, without inflow of

[5] Note that the initial kinetic energy of injected pairs is much less than the energy of the pair producing photons; this is easy to see from equation (17). The rest of the energy goes into synchrotron radiation; that energy is carried by many photons with energies much less than that of the primary photon.
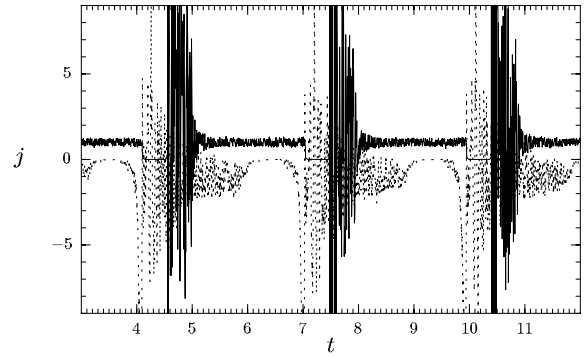

Figure 8. Currents through the domain boundaries for cascade with $j_\mathrm{m} = j_\mathrm{GJ}$ as functions of time for three consecutive bursts of pair formation. The current flowing into the magnetosphere is shown by the solid line. The current flowing *into* the NS is shown by the dashed line (note that the direction for this current is opposite to the current direction assumed in the rest of the paper, so it should be on average negative). Currents are normalized to the GJ current j_GJ. The currents are averaged over 10 timesteps.

charged particles from the magnetosphere [the latter mechanism of current adjustment has been discussed in Lyubarskij (1992) and Timokhin (2006)].

In Fig. 8 I plot electric currents through the lower domain boundary towards the NS surface (dashed line; this current should be negative) and through the upper end of the calculation domain (solid line; this current should be positive) as functions of time. The required current density j_m is achieved on average, at each moment of time the current density deviates from j_m. Fluctuations are the strongest when particles from the burst of pair formation hit the NS surface, and when the blob reaches the outer boundary. In all cases the relative deviation of the mean over the cycle current density from j_m is less than $\sim 10^{-3}$.

4.4 Cascade energetics

The height of the gap is nearly two times larger than the estimate given by equation (22). The reason for this is that the upper boundary of the vacuum gap – the end of the blob tail – is moving into the magnetosphere while the electrons which ignite the cascade are moving towards the NS. When these electrons arrive at the point where they emit first pair-production capable photons, the gap's upper boundary has moved some distance into the magnetosphere and the gap size is larger.

The electric field in the gap linearly increases towards the NS and the first secondary particles are injected into the region with very strong electric field. A substantial amount of particles need to be generated before the vacuum electric field is screened. In the meanwhile the vacuum gap is still growing and freshly injected particles are accelerated in a very strong electric field. In the considered case a noticeable number of particles reach the radiation-reaction limited Lorentz factor $\sim 1.4 \times 10^7$ (see snapshots at $t = 6.8$, 6.95 in Fig. 4). This energy is nearly four times higher than $\gamma_\mathrm{RS,1}^\mathrm{max}$ given by equation (24). When the electric field is screened these particles start losing their energy quickly and then for the most of the pair-producing positrons the Lorentz factor does not exceed $\gamma_\mathrm{L} \sim 8 \times 10^6$ (see snapshots at $t = 7.1$, 7.25 in Fig. 4). γ_L is the Lorentz factor of a relativistic electron/positron which lose substantial amount of its kinetic energy due to curvature radiation while moving a distance comparable to the length of the computation domain: $\gamma_\mathrm{L}/\delta t \sim W_\mathrm{rr}$; $\delta t = L/c$ and W_rr is the radiation-reaction term in the equation of
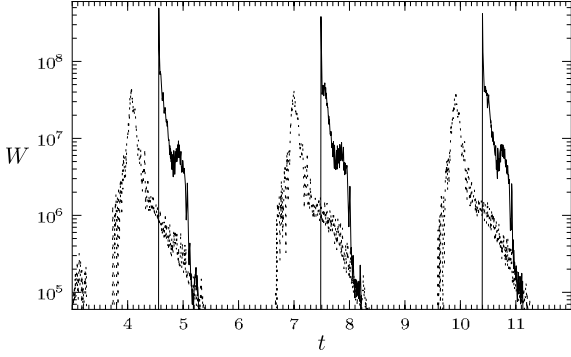
Figure 9. Energy fluxes through the domain boundaries for cascade with $j_m = j_{GJ}$ as functions of time for three consecutive bursts of pair formation. The flux towards the magnetosphere is shown by the solid line; the flux towards the NS is shown by the dashed line. Fluxes are normalized to $m_e c^2 n_{GJ} c$ and are averaged over 10 time-steps.

motion (5); it is given by equation (6). In terms of the problem's parameters

$$\gamma_L \sim 5.6 \times 10^4 \rho_6^{2/3} \left(\frac{L}{c}\right)^{-1/3} \sim 8 \times 10^6 \; ; \tag{26}$$

it is still nearly two times larger than $\gamma_{RS,1}^{max}$ given by equation (24). The particle energy distribution at high energies is quite flat (see Fig. 6). So, pair-producing particles are more energetic than it is expected from simple estimates. Because of these the total number of pairs generated by a *single* burst of pair formation should be larger than that assumed in 'standard' Ruderman–Sutherland model. In order to get the final pair multiplicity detailed full cascade simulations are necessary, which will be the subject of a separate research. The total number of high-energy particles with $\gamma > 5 \times 10^5$ in a blob is $\sim 0.7\, n_{GJ} r_{pc}$ per cm^2 of the blob perpendicular cross-section.

In Fig. 9 I show energy fluxes trough the lower and upper boundaries of the calculation domain as functions of time. The energy flux hitting the NS surface is shown by the dashed line; the energy flux going into the magnetosphere – by the solid line. The fluxes are normalized to $m_e c^2 n_{GJ} c$; they are computed by summing kinetic energies of all particles leaving the domain at every time-step. These functions have spikes when secondary particles accelerated at the early stage of blob formation pass trough the corresponding boundaries. The energy carried by particles in the blob tail is negligible (intervals between the spikes) and so the energy is deposited only during bursts of pair formation. The energy flux into the magnetosphere is larger because most of the secondary electrons slam into the NS surface before they achieve the maximum possible energy while secondary positrons can gain the maximum energy as they fly away from the surface. The mean energy flux going towards the NS averaged over the duration of the spike, e.g. over $t \in [6.6, 8]$ in Fig. 9, is $\sim 4 \times 10^6 m_e c^2 n_{GJ} c$; the flux going into the magnetosphere averaged over the same time is $\sim 8 \times 10^6 m_e c^2 n_{GJ} c$. If the time between two successive discharges is $(r_{pc}/c)f$ (i.e. the time between discharges is f times larger than polar cap flyby time) the average energy flux going into heating of the NS is $\sim 1.5 \times 10^{22} f^{-1}$ erg s^{-1} cm^2; this would result in the polar cap temperature $T_{pc} \sim 4 \times 10^6 f^{-1/4}$ K, if the heat conductivity is neglected. The flux going into the magnetosphere is $\sim 3 \times 10^{22} f^{-1}$ erg s^{-1} cm^2. Obviously, when the time between successive bursts of pair formation is large, the overall heating of the NS surface is significantly reduced.

4.5 Cascades with $j_m = 0.5, 1.5 j_{GJ}$

When the current density in the cascade zone is different from the GJ current density plasma flow is qualitatively similar to the case $j_m = j_{GJ}$ described above. In Figs 10 and 11, I show snapshots of change density distribution and detailed characteristics of cascade with $j_m = 0.5 j_{GJ}$; in Figs 12 and 13 – the same plots for cascade with $j_m = 1.5 j_{GJ}$. The sizes of computational domains are the same as in the case of $j_m = j_{GJ}$, so the time t in these plots, normalized to the flyby time, is measured in the same units. The time intervals between individual plots in Figs 10 and 12 are the same as in Fig. 2 discussed before. Note, however, that snapshots in Figs 4, 11 and 13 are taken at different phases of the pair formation cycle. In all cases discharges repeat quasi-periodically and creation of pair plasma goes through the same three phases: vacuum gap formation ($t = 5.8–7$ for $j_m = 0.5 j_{GJ}$; $t = 5.483–6.083$ for $j_m = 1.5 j_{GJ}$), formation and propagation of the plasma blob ($t = 7–8.2$ for $j_m = 0.5 j_{GJ}$; $t = 6.083–7.283$ for $j_m = 1.5 j_{GJ}$) and relaxation ($t = 8.2–8.6$ for $j_m = 0.5 j_{GJ}$; $t = 7.283–8.283$ for $j_m = 1.5 j_{GJ}$). The structure of the plasma blob is similar – there is a charged sheath screening plasma in the blob from the large electric field in the vacuum gap, and there are large amplitude plasma oscillations in the blob. The superluminal plasma waves are also present.

Cascade parameters for the case $j_m = 0.5 j_{GJ}$ differ from those for the case $j_m = j_{GJ}$ as follows. The size of the plasma blob is larger. The velocity of the previous blob's tail is smaller, $v_{tail} \sim 0.44c$, and the vacuum gap shrinks faster – one can see its disappearance in timeshots at $t = 7.017–7.517$ (Figs 10 and 11). When the gap closes, the charge sheath at the blob front edge disappears and there is no additional particle acceleration there – in Fig. 10 at $t = 7.467$ the sheath is still present, at $t = 7.567$ it disappears. The maximum particle energy is smaller – particles do not reach the radiation-reaction limited energy – but their maximum energy after the electric field is screened is the same γ_L given by equation (26). The plasma density in the blob is nearly four times smaller. The total number of high-energy particles with $\gamma > 5 \times 10^5$ in the blob is $\sim 0.22\, n_{GJ} r_{pc}$ per cm^2 of the blob perpendicular cross-section, which is ~ 3.5 times smaller than in the case $j_m = j_{GJ}$. The energy flux towards the NS is, as expected, smaller, $5.8 \times 10^{21} f^{-1}$ erg s^{-1} cm^2, and the estimated temperature of the polar cap is lower, $T_{pc} \sim 3.2 \times 10^6 f^{-1/4}$ K.

Cascade parameters for the case $j_m = 1.5 j_{GJ}$ differ from those for the case $j_m = j_{GJ}$ as follows. The size of the plasma blob is smaller. The velocity of the previous blob's tail is $v_{tail} \sim 0.82c$; it is smaller than that in the case of $j_m = j_{GJ}$, but it is significantly larger than v_{tail} for the case $j_m = 0.5 j_{GJ}$. Although the gap shrinks faster it still leaves the domain. First-generation secondary particles reach the radiation-reaction limited energy and then slow down to the Lorentz factors $\lesssim \gamma_L$. The plasma density in the blob is slightly higher. The total number of high-energy particles with $\gamma > 5 \times 10^5$ in the blob is $\sim 0.6\, n_{GJ} r_{pc}$ per cm^2 of the blob perpendicular cross-section, which is slightly less than that value for $j_m = j_{GJ}$ cascade. The energy flux towards the NS is slightly lower, $\sim 1.3 \times 10^{22} f^{-1}$ erg s^{-1} cm^2, and the estimated temperature of the polar cap $T_{pc} \sim 3.9 \times 10^6 f^{-1/4}$ K.

These differences are ultimately related to the speed at which the tail of the previous blob leaves the domain and number of electrons leaking from it. The cascade energetics and the ultimate pair multiplicity depend on the number of the first-generation secondary positrons, their maximum energy and for how long these particles are sustained at this energy. The first-generation secondary particles are accelerated up to very high energies – they can be accelerated
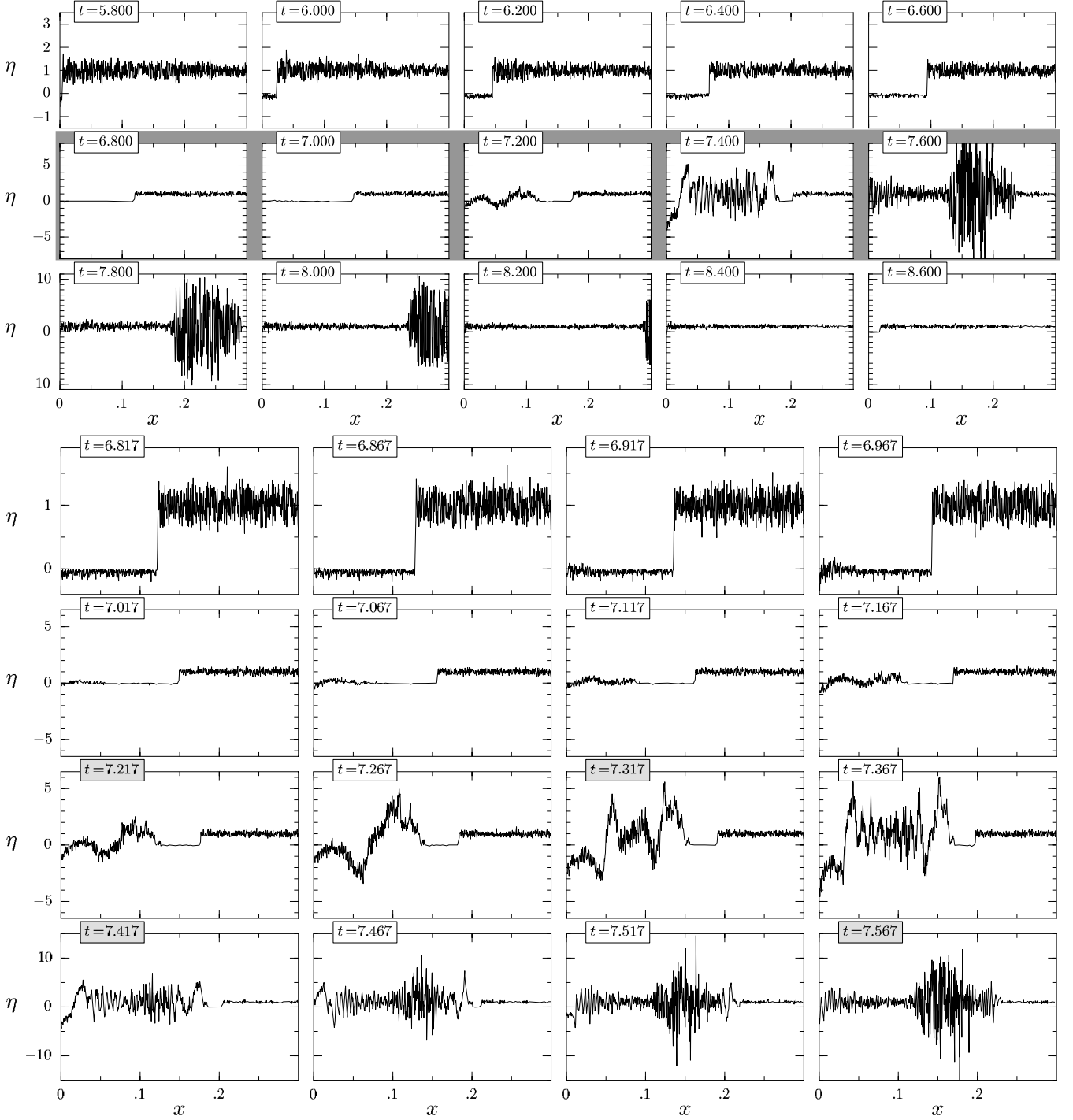
Figure 10. Snapshots of charge density distribution in the calculation domain for cascade with $j_m = 0.5 j_{GJ}$. The same notations are used as in Fig. 2.

up to the radiation-reaction limited energy – and are sustained at this energy until enough plasma is produced to screen the electric field in the blob. The rate of the first-generation secondary positrons production depends on how many electrons leak from the tail of the previous blob, and the maximum energy of these positrons depends on the electric field where they are injected – the faster the gap grow the larger the electric field.

In the case $j_m = j_{GJ}$ redistribution of particle momenta is not necessary for the adjustment of the current density – bulk motion of the tail towards the magnetosphere would provide the required current density because the charge density is already η_{GJ}; so in this case the average speed of the tail is the largest. The gap grows fast, and the first generation of secondary particles is created in a region with very strong electric field. When the current density j_m differs from the GJ current density, redistribution of particle momenta is required to sustain j_m by keeping at the same time the charge density equal to the GJ charge density. For $j_m > j_{GJ}$ electrons must be sent back to increase the current, for $j_m < j_{GJ}$ some positrons must be reversed to decrease the current. The plasma as whole moves into the magnetosphere; low-energy particles are
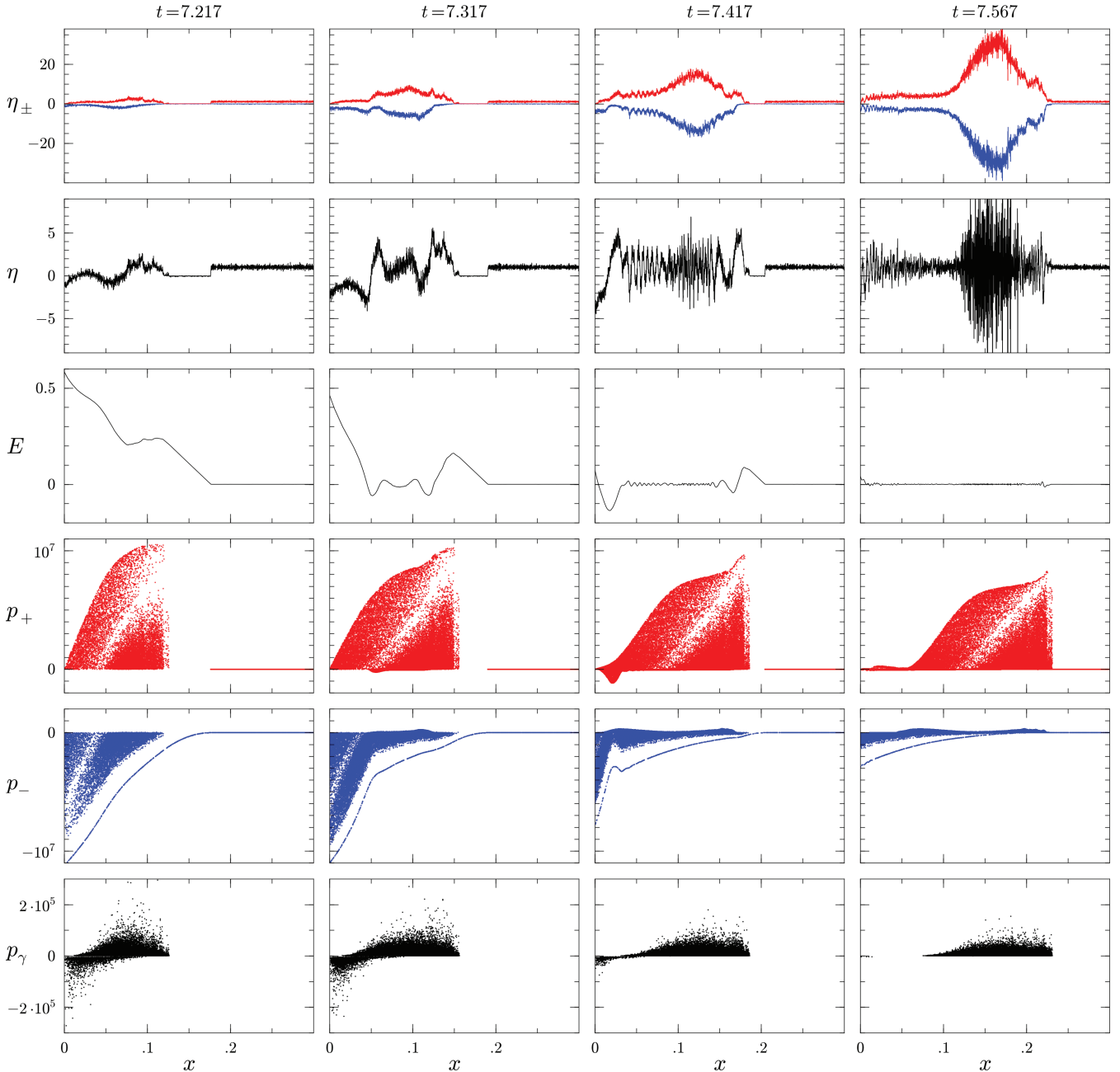
Figure 11. Screening of the electric field in cascade with $j_m = 0.5j_{GJ}$. Snapshots are take at the same time moments as the marked snapshots in the bottom panel of Fig. 10. The same quantities are plotted as in Fig. 3.

trapped in small amplitude plasma oscillations and are dragged with the bulk of the plasma. The presence of a weak electric field would be sufficient to ensure that the required number of particles on average moves towards the NS. Such particle reversal results in slower motion of the tail. When the gap upper boundary moves slowly, the first generation of secondary particles is injected in a weaker electric field, and the overall energetics of cascade is lower. On the other hand, the larger the current density the larger the number of electrons leaking from the tail; these electrons are the primary particles igniting the cascade. To screen the electric field at least GJ number density of particles is required. When the flux of the primary electrons is higher, the number of the first-generation secondary pairs grows faster, and polarization of the plasma which

can screen the vacuum electric field is achieved at smaller spacial separation; this results in a smaller size of the plasma blob. So, cascades with the current density equal to the GJ current density are most energetic and should produce densest plasma. However, as it follows from the simulations, for $j_m > j_{GJ}$ cascade properties seem to be less sensitive to the value of j_m than properties of cascades with $j_m < j_{GJ}$. Hence, cascades with $j_m > j_{GJ}$ should have energetics and final multiplicities lower but comparable to those of cascades with $j_m = j_{GJ}$, while energetics and final multiplicities of cascades with $j_m < j_{GJ}$ should be significantly lower.

In Figs 14 and 15 I plot electric currents through the lower and upper domain boundaries for cascades with $j_m = 0.5j_{GJ}$ and $j_m = 1.5j_{GJ}$ correspondingly. Except for the value of the mean current
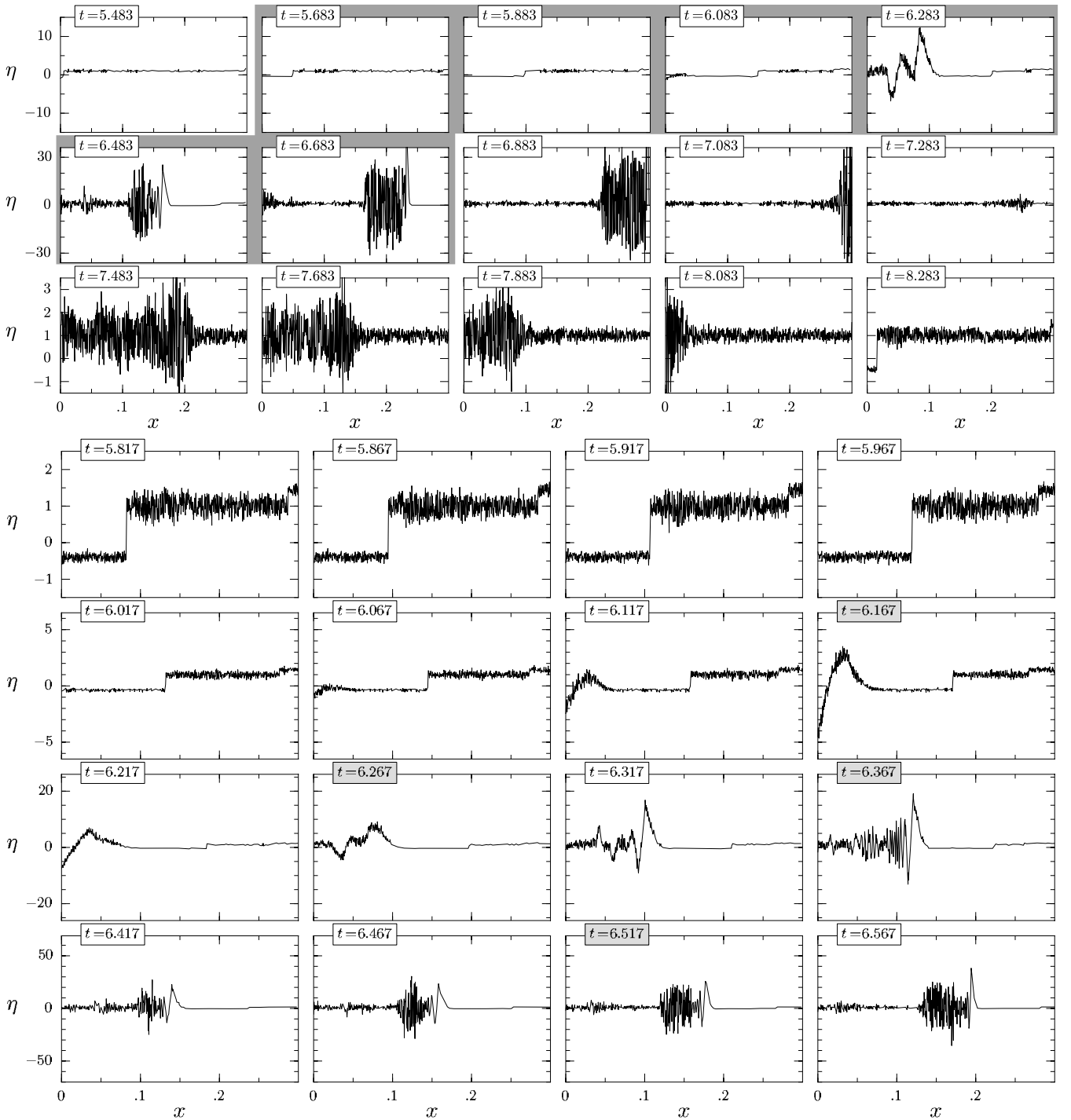
Figure 12. Snapshots of charge density distribution in the calculation domain for cascade with $j_{\rm m} = 1.5 j_{\rm GJ}$. The same notations are used as in Fig. 2.

density these currents behave in a similar way as the currents for a cascade with $j_{\rm m} = j_{\rm GJ}$; the relative deviation of the mean over the cycle current density from $j_{\rm m}$ is also less than $\sim 10^{-3}$.

Regarding the repetition rate of pair formation bursts in cascades with different current densities I can make only some qualitative remarks. For cascades with smaller $j_{\rm m}$s pair multiplicity is smaller, which must result in a less dense plasma tail; there will be less particles to wipe out of before the next vacuum gap can develop. On the other hand, if the current density is smaller, particles are wiped out slower because smaller current density requires less par-

ticles to sustain it. For cascades with higher current densities pair multiplicity should be higher, but a larger particle flux is required. So, it seems that dependence of the time between the discharges on the current density should be moderate; it is also possible that this dependence is non-monotonic.

4.6 Summary of cascade properties

The case described in details in the previous sections is a good example of a typical Ruderman–Sutherland cascade. Insights gained
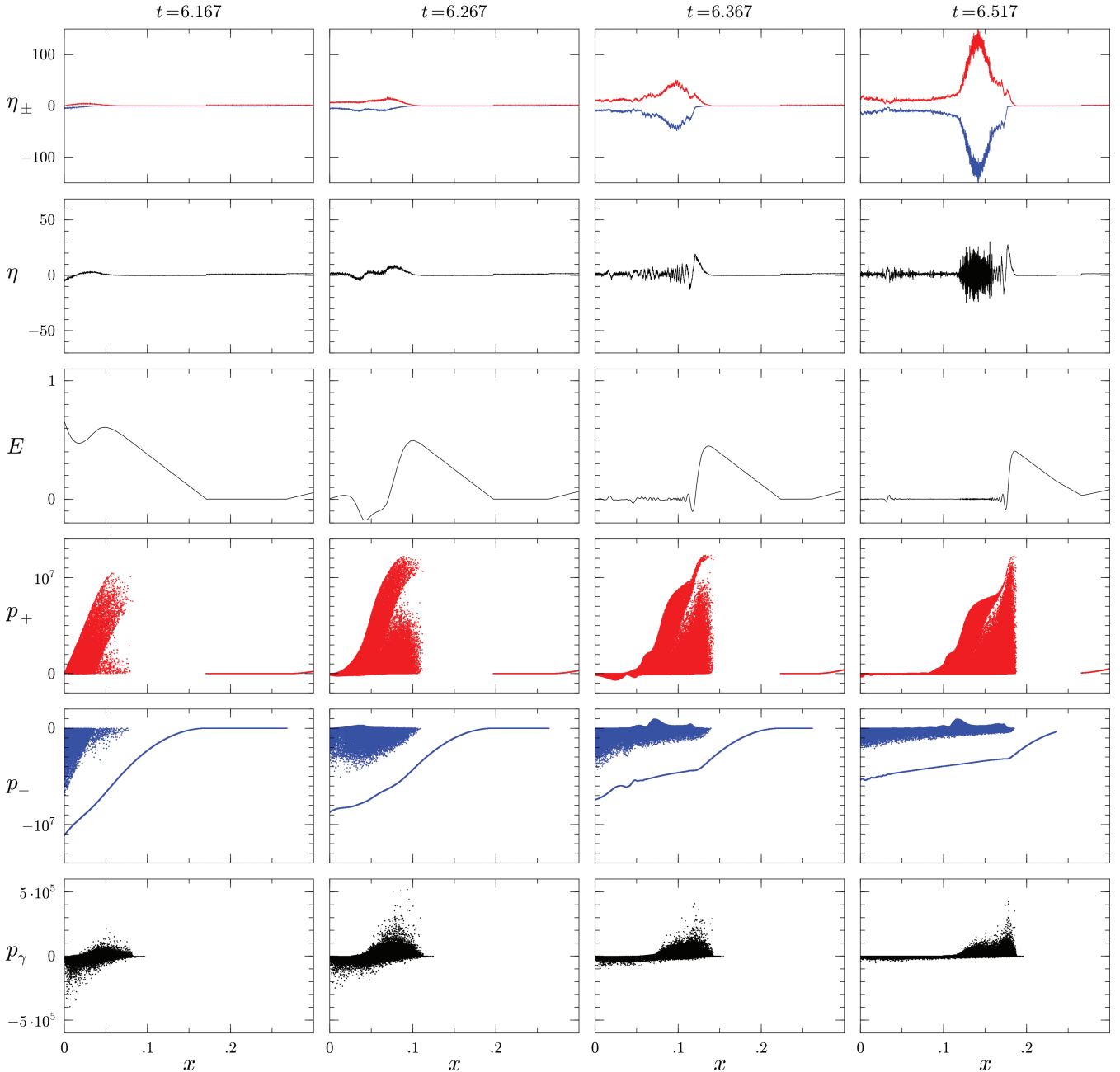
Figure 13. Screening of the electric field in cascade with $j_m = 1.5j_{GJ}$. Snapshots are taken at the same time moments as the marked snapshots in the bottom panel of Fig. 12. The same quantities are plotted as in Fig. 3.

from analysing that case helped to draw a general physical picture. I performed simulation for different pulsar parameters (P, B_0, ρ), and the results are in complete agreement with the general picture outlined below.

Cascades show limit cycle behaviour for all physical parameters allowing pair creation. Pair formation is quite regular – in each discharge a blob of pair plasma is formed; the blob propagates into the magnetosphere leaving behind a tail of low-energy particles. When particle number density in the tail becomes comparable to n_{GJ} a vacuum gap appears, and then a new blob of pair plasma forms. There are two characteristic time-scales: (i) time-scale associated with the size of the plasma blob $\tau_1 = L_{blob}/c$, and (ii) time between two successive discharges τ_2. The first time-scale is of the order

of $\tau_1 \sim h_{RS}/c$ for all j_m, and it should be (much) smaller than the second time-scale, $\tau_1 \ll \tau_2$. The simulations are inconclusive about the real dependence of τ_2 on the current density j_m, but it seems that this dependence might be weaker than linear.

When a new burst of pair creation occurs, the vacuum gap detaches from the NS surface and propagates into the magnetosphere. The upper boundary of the gap moves subrelativistically, while the front of the new blob moves ultra-relativistically; eventually the gap closes. For sub-GJ current densities the tail of the previous blob moves slower and the gap disappears faster. For cascades with super-GJ current densities the gap should disappear faster for larger values of j_m, but the dependence of the tail velocity v_{tail} on j_m is significantly weaker than that in cascades with sub-GJ current
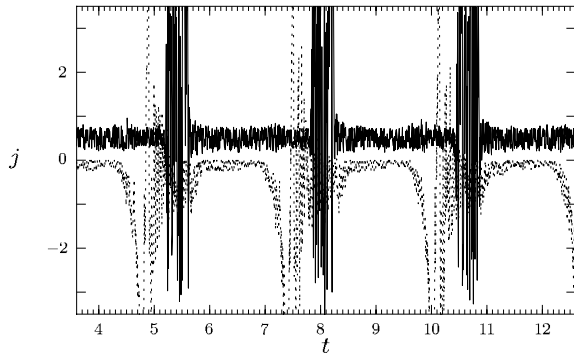
Figure 14. Currents through the domain boundaries for cascade with $j_{\mathrm{m}} = 0.5 j_{\mathrm{GJ}}$ as functions of time for three consecutive bursts of pair formation. The currents are averaged over 10 time-steps. The same notations are used as in Fig. 8.

Figure 15. Currents through the domain boundaries for cascade with $j_{\mathrm{m}} = 1.5 j_{\mathrm{GJ}}$ as functions of time for three consecutive bursts of pair formation. The currents are averaged over 10 time-steps. The same notations are used as in Fig. 8 .
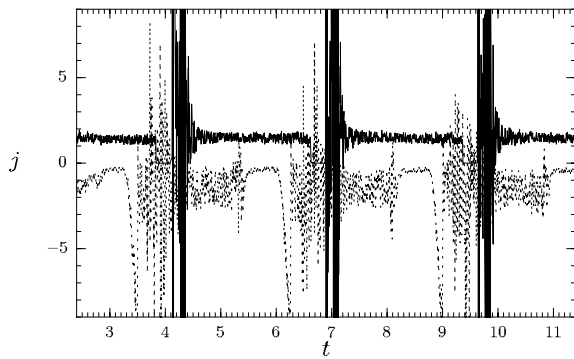
densities. The gap should persist for longest time in cascades with $j_{\mathrm{m}} = j_{\mathrm{GJ}}$.

For pulsars with large potential drop across the gap the first generation of pairs in cascades with $j_{\mathrm{m}} \gtrsim 0.5 j_{\mathrm{GJ}}$ reaches the radiation-reaction limited energy. When electric field is screened, these particles propagate losing their energy by emitting curvature photons. At first these losses are large, as radiation efficiency depends on particle energy as $\propto \gamma^4$, but then particles lose energy more slowly. There is also a small amount of particles in the charge sheath at the front of the plasma blob which feel the non-screened electric field and are continuously accelerated. For current densities $j_{\mathrm{m}} \lesssim 0.5 j_{\mathrm{GJ}}$ particles do not reach radiation-reaction limited energies. However, in any case the kinetic energy of the first-generation particles is larger than it follows from estimates of Ruderman & Sutherland (1975) and so the final pair multiplicity and energetics of a *single* bust of pair formation are higher. The vast majority of energy is carried by the first-generation pairs and so the heating of the NS polar cap by the cascade occurs in bursts, when first-generation pair electrons hit the surface; heating during the 'relaxation' phase is negligible. If the time between successive discharges is large, the heating will be much lower than it is usually assumed in the Ruderman–Sutherland model.

During the discharge a superluminal electrostatic wave is formed. As its phase velocity is larger than the speed of light it is not damped via the Landau damping. From the performed simulations the ultimate fate of this wave is not clear because after some time the code stops resoling its wavelength.

5 DISCUSSION

I performed for the first time self-consistent time-dependent modelling of electromagnetically driven cascades which included all essential physical processes. I considered the simplest possible case – the Ruderman–Sutherland cascade, when all particles in the discharge zone are produced by the cascade itself. Cascade behaviour is quite regular – spatially localized blobs of pair plasma are formed during regularly repeating discharges; each blob propagates into the magnetosphere leaving a tail of mildly relativistic plasma behind. Energetics of individual discharges is higher than that predicted by the Ruderman–Sutherland model.

The model is 1D and includes the minimum set of processes involved; but just because a 'bare-bone' system was considered it was possible to get insights about general physics of electromagnetically driven cascades. I was interested in dynamics of electromagnetic discharges, i.e. how particles are accelerated when pair production takes place. I did not follow the development of the full cascade initiated by energetic particles moving in the magnetosphere above the polar cap where there is no accelerating electric field. The latter problem has been studied before by many authors, and qualitative properties of cascades initiated by a relativistic particle are relatively well known (e.g. Daugherty & Harding 1982; Zhang & Harding 2000; Hibschman & Arons 2001b; Medin & Lai 2010). In future works I plan to address this problem using particle energy distributions obtained from self-consistent discharge simulations. Although quantitatively results of such full cascade simulations would be different from that described in the above mentioned papers, qualitatively they should be similar.

In my 1D simulations, individual discharges are very similar and electrostatic oscillations are clearly visible and coherent. Usually 1D and 2D models show more coherent behaviour than full 3D simulations because of the inforced symmetry. Hence, the coherent behaviour present in this 1D simulations could be somewhat washed out in a more realistic 3D model. The usual picture used in models of polar cap discharges involves several separate discharge zones across the polar cap – 'sparks' in terms of the Ruderman–Sutherland model. Whether interaction between sparks via induced electric field is strong enough for them to be coupled is a priori not clear. However, particle motion in the superstrong magnetic field in the pulsar polar cap is 1D, the curvature of magnetic field lines is small and photon trajectories only slightly deviate from particles trajectories; this suggests that most of the cascade properties deduced from current simulations can be preserved in a full 3D model for individual sparks, although only direct 3D simulations can prove this.

I considered the case when particles cannot be extracted from the surface of the NS, but the results may be applicable to a broader class of problems. If cascades under different physical conditions work as a series of discharges, their behaviour should be similar to that described here. Namely, the blob-tail structure can be preserved, pair plasma thermalization will take place and transient electrostatic wave will be excited. In particular, I suspect that polar cap cascades with space charge limited flow – in a non-stationary version of the model suggested by Arons & Scharlemann (1979) and Muslimov & Tsygan (1992) – might have some similarities with the case described here.

One of the main motivations to start this project was to study how cascade zone provides the current density required by the

magnetosphere. It has been speculated that non-stationary cascade can be sustained at any average current density flowing through the discharge zone (e.g. Levinson et al. 2005; Timokhin 2006). My simulations have explicitly shown that this is indeed the case. The current density at any given point fluctuates strongly, but on average it is equal to the mean current density j_m with very high accuracy. Current adjustment works well in the relaxation phase too, when both the charge and the current densities are close to the required values even when they are averaged over time-scales much smaller than the flyby time of the calculation domain. It works because in the tail there are low-energy particles trapped in small amplitude plasma oscillations, and the weak fluctuating electric field of plasma oscillations is able to reverse particles of *both signs* (at different oscillation phases). Particles which flow backwards do it in time-averaged sense; they spend more time in backward motion; there is no separate population of particles flowing only backwards all the time. Such way of current adjustment is possible because of effective plasma thermalization which provides low-energy particles.

The current density j_m can have the sign opposite to the sign of the GJ charge density, $j_m < 0$ (Timokhin 2006). I ran simulations with $j_m < 0$ too; everything works exactly in the same way as in the case with $j_m > 0$, except that the gap forms at the upper domain boundary, at the magnetosphere side. This 1D problem is symmetric with regard to the sign of the current density: if $j_m < 0$, the pair plasma – which has positive net charge in order to sustain the GJ charge density – moves towards the NS and generates negative j_m. However, at the magnetosphere side there is no solid surface which can prevent charged particles from escaping; if a gap forms there, some charged particles can be sucked from the magnetosphere. In principle, it might result in the presence of particles of both signs in the gap and, therefore, in cascade ignition at both ends of the gap; whether this is the case or not cannot be decided based solely on qualitative arguments and requires accurate quantitative modelling. The gap will form in the tail of the blob tearing it apart; this will happen at distances from the NS surface larger than the polar cap size, and so the problem cannot be adequately described by the used 1D approximation. The case of $j_m < 0$ will be addressed in a later work. Qualitatively, however, it seems that any cascade operating as a series of discharges would produce a population of low-energy particles, and so it should be able to adjust to any current density in the way described above, if enough charged particles are generated.

The simulations are inconclusive about how long the thermalization persists, because I cannot follow the plasma blob for a long time. It definitively works during the blob formation. For as long as there are low-energy particles in the blob the current adjustment will work as described above. Note that for current adjustment the number density of low-energy particles should be comparable to n_{GJ}, which is only a very small fraction of the plasma density in the blob. If, however, at some time the blob runs out of low-energy particles, a macroscopic electric field will arise which can adjust the current density by creating a separate population of backward moving particles or/and shifting mean velocities of electrons and positrons as suggested in e.g. Scharlemann (1974) and Lyubarsky (2009).

I performed a full-fledged kinetic modelling of pair cascades including all essential classes of physical processes relevant to dynamics of electromagnetically driven cascades, listed at the beginning of Section 2. All previous attempts to model time-dependent cascades used on-the-spot approximation for pair injection. In some works fluid approximation has been used, where electrons and positrons were represented as fluids (Levinson et al. 2005; Luo & Melrose 2008). Although the physical situation I considered – the Ruderman–Sutherland cascade in the polar cap – is different from ones studied in the previous works, it is possible to assert applicability of on-the-spot and two-fluid approximations in a general context, based on the general picture of cascade development inferred from my simulations.

It turns out that the delay of pair injection due to finite time necessary for a photon to propagate before it is absorbed does not introduce new qualitative features. I also performed simulations using on-the-spot approximation, when an electron–positron pair was injected at the position and at time where and when the parent particle emitted the pair producing photon. Quantitatively, on-the-spot approximation introduces error in final energies of the relativistic particles and all depending on them cascade parameters by a factor of several. However, qualitatively, the results are similar, i.e. the pattern of the plasma flow remains the same: pair formation is quasi-periodic with plasma blobs propagating into the magnetosphere leaving tails of modestly relativistic particles.

In the first work about modelling of time-dependent cascades by Al'Ber et al. (1975) a zero-dimensional model was used – only temporal, but not spatial, variations in particle number density were considered. In that model, the production of larger amount of particles than necessary for screening of the electric field was due to the time delay between the photon emissions and absorptions. As all later attempts to model time-dependent cascades used on-the-spot approximations for pair injections (Levinson et al. 2005; Beloborodov & Thompson 2007; Luo & Melrose 2008), the question about the importance of pair injection delay remained unanswered. In my simulations the overshooting in pair number density arises mainly because of the spatial separation between the acceleration and the pair-production zones in a quite regular plasma flow. Particles are accelerated in the gap and must travel some distance before they can emit high-energy photons. There are particles of only one charge sign in the gap, and so pairs are injected at only one end of the gap. There always exists a spatial domain with the electric field (the gap) where pairs cannot be injected and the electric field is not regulated directly by the pair injection. The back reaction on the electric field proceeds only by means of gap shrinkage, which is slow. This causes an overshooting in pair production and so the intermittency of pair creation. Inclusion of spatial and temporal delays of pair injection due to photon propagation only exaggerates this effect, but it does not introduce a new kind of behaviour. Hence, using on-the-spot approximation in toy models seems to be justified. On the other hand, in a situation when plasma flow can become chaotic the time delay might become a deciding factor for the creation of plasma density overshoot.

Two-fluid approximation, on the other hand, is inadequate. The pair plasma in the discharge zone acquires a large momentum dispersion and some particles become mildly relativistic. A weak fluctuating electric field easily reverts particles of both signs and plasma becomes essentially four-component (see Section 4.3). In two-fluid approximation at any given point at any time each particle specie (electrons and positrons) can move only in one direction. This introduces an additional rigidity, which might be the reason why Levinson et al. (2005) got strong fluctuating electric field throughout the whole domain. Although I considered a different physical situation and the results described in this paper cannot be directly compared with the results of Levinson et al. (2005) and Luo & Melrose (2008), I think that the latter are seriously flawed by the use of two-fluid approximation.

Now I would like to discuss how properties of cascades could manifest in pulsar radioemission. Pair creation is not chaotic, with clear signatures of a limit cycle behaviour; this ought to have strong

observational implications. If, as it is widely accepted today, pulsar radioemission is directly related to pair production, the periodicity of cascades must be visible in power spectra of pulsar individual pulses. There are two characteristic time-scales: τ_1, associated with the blob size, and τ_2, the time between discharges. The size of the blob to the order of magnitude is approximately the same for all current densities, and so τ_1 is of the same order for any reasonable current density j_m; τ_2, on the other hand, should be more variable.

Pulsar radioemission is highly variable on time-scales comparable with the pulsar period: emission occurs mainly in the form of subpulses, in some pulsars subpulses drift, some pulsars change modes and/or switch off for many periods. This hints that current density can fluctuate because of some processes involving the whole magnetosphere (e.g. Arons 1983; Timokhin 2010). Cascades can adjust to any reasonable current density, and so the current density at a fixed colatitude might vary on time-scales much larger than τ_1, τ_2; on the other hand, the current density varies across the pulsar polar cap anyway. Because of these, an individual subpulse represents emission averaged over time and space, or, in other words, over a range of different j_ms, and so the features of cascades along separate field lines will be smeared. Hoverer, the time-scale associated with the size of plasma blob τ_1 by the order of magnitude remains the same and should be clearly visible in the power spectrum. The second time-scale τ_2 should be less prominent, but, as discussed before, it might not be extremely sensitive to the current density, and, therefore, it might manifest as a broad feature in the power spectrum.

The blob is of the same length as the region with the accelerating electric field. In the Ruderman–Sutherland model this length is small, and the corresponding time-scale τ_1 is less than a microsecond. In space charge limited flow models, on the other hands, the length of the acceleration zone should be comparable to the NS radius; if in this case cascades work similarly, τ_1 should be of the order of $\sim 100\,\mu s$. The second time-scale, τ_2, should be substantially longer, a factor from a few to hundreds. There is evidence of different characteristic time-scales in pulsar microstructure, from nano- to milliseconds; in some pulsars microstructure is also quasi-periodically modulated (e.g. Boriakoff 1976; Popov et al. 2002). It is not clear whether microstructure time-scales are due to polar cap cascades variability or not, but τ_1, τ_2 can be in the range of observed microstructure modulation times, and cascades operating as a series of discharges should have double time-scale signature.

The problem of pulsar radioemission mechanism in notoriously difficult and currently there is no reliable theory which could adequately explain it. The firmly established observational fact about pulsar radioemission is that it is due to some collective process. In my simulations I saw formation of a large amplitude electrostatic wave. Its phase velocity is larger than the speed of light, and it is not damped via the Landau damping. In 1D in a superstrong magnetic field only electrostatic waves exist, but in a real pulsar such wave can be coupled to an electromagnetic mode; if it stays superluminal, it can escape the magnetosphere. This wave is a collective form of emission, as it involves coherent macroscopic plasma motion. The simulations are inconclusive about the fate of that wave because at some point the numerical scheme stops resolving its wavelength; it is also not clear how coherent the whole picture is in 3D. May be it is too preliminary to tell whether pulsar radioemission, or some of its component, is related to this transient wave, but in future research special attention should be paid to such transient waves.

REFERENCES

Al'Ber Y. I., Krotova Z. N., Eidman V. Y., 1975, Astrophys., 11, 189
Arons J., 1983, in Burns M. L., Harding A. K., Ramaty R., eds, AIP Conf. Ser. Vol. 101. Positron–Electron Pairs in Astrophysics. Am. Inst. Phys., New York, p. 163
Arons J., 2009, in Becker W., ed., Astrophys. Space Sci. Libr. Vol. 357, Neutron Stars and Pulsars. Springer, Berlin, p. 67
Arons J., Scharlemann E. T., 1979, ApJ, 231, 854
Bai X., Spitkovsky A., 2010, ApJ, 715, 1282
Beloborodov A. M., Thompson C., 2007, ApJ, 657, 967
Beskin V. S., 1990, Pis ma Astron. Zh., 16, 665
Beskin V. S., Istomin Y. N., Parev V. I., 1992, SvA, 36, 642
Birdsall C., Langdon A., 1985, Plasma Physics via Computer Simulation. McGraw-Hill, New York
Boriakoff V., 1976, ApJ, 208, L43
Cheng A., Ruderman M., Sutherland P., 1976, ApJ, 203, 209
Cheng K. S., Ho C., Ruderman M., 1986, ApJ, 300, 500
Contopoulos I., Kazanas D., Fendt C., 1999, ApJ, 511, 351
Daugherty J. K., Harding A. K., 1982, ApJ, 252, 337
Erber T., 1966, Rev. Modern Phys., 38, 626
Fawley W. M., 1978, PhD thesis, AA (California Univ., Berkeley)
Fishman G. S., 1996, Monte Carlo: Concepts, Algorithms, and Applications. Springer, New York
Gold T., 1969, Nat, 221, 25
Goldreich P., Julian W. H., 1969, ApJ, 157, 869
Gruzinov A., 2005, Phys. Rev. Lett., 94, 021101
Harding A. K., Muslimov A. G., 2002, ApJ, 568, 862
Hewish A., Bell S. J., Pilkington J. D. H., Scott P. F., Collins R. A., 1968, Nat, 217, 709
Hibschman J. A., Arons J., 2001a, ApJ, 554, 624
Hibschman J. A., Arons J., 2001b, ApJ, 560, 871
Hirotani K., Okamoto I., 1998, ApJ, 497, 563
Jackson J. D., 1975, Classical Electrodynamics. Wiley, New York
Kalapotharakos C., Contopoulos I., 2009, A&A, 496, 495
Krause-Polstorff J., Michel F. C., 1985, MNRAS, 213, 43 P
Levinson A., Melrose D., Judge A., Luo Q., 2005, ApJ, 631, 456
Luo Q., Melrose D., 2008, MNRAS, 387, 1291
Lyubarskij Y. E., 1992, A&A, 261, 544
Lyubarsky Y., 2009, ApJ, 696, 320
Medin Z., Lai D., 2007, MNRAS, 382, 1833
Medin Z., Lai D., 2010, MNRAS, 406, 1379
Melrose D. B., Rafat M. Z., Luo Q., 2009, ApJ, 698, 115
Mestel L., 1999, Stellar Magnetism. International Series of Monographs on Physics. Clarendon, Oxford, p. 99
Muslimov A. G., Tsygan A. I., 1990, SvA, 34, 133
Muslimov A. G., Tsygan A. I., 1992, MNRAS, 255, 61
Pacini F., 1967, Nat, 216, 567
Popov M. V., Bartel N., Cannon W. H., Novikov A. Y., Kondratiev V. I., Altunin V. I., 2002, A&A, 396, 171
Ruderman M. A., Sutherland P. G., 1975, ApJ, 196, 51
Scharlemann E. T., 1974, ApJ, 193, 217
Sobol' 1973, Numerical Monte-Carlo Methods. Nauka, Moscow
Spitkovsky A., 2006, ApJ, 648, L51
Sturner S. J., Dermer C. D., Michel F. C., 1995, ApJ, 445, 736
Sturrock P. A., 1971, ApJ, 164, 529

Thompson C., 2008, ApJ, 688, 499
Timokhin A. N., 2006, MNRAS, 368, 1055
Timokhin A. N., 2007a, MNRAS, 379, 605
Timokhin A. N., 2007b, Ap&SS, 308, 575
Timokhin A. N., 2009, preprint (arXiv:0912.5475)
Timokhin A. N., 2010, MNRAS, 408, L41
Verboncoeur J. P., 2005, Plasma Phys. Controlled Fusion, 47, A260000
Villasenor J., Buneman O., 1992, Comput. Phys. Comm., 69, 306
Zhang B., Harding A. K., 2000, ApJ, 532, 1150

APPENDIX A: ONE-DIMENSIONAL TIME-DEPENDENT ELECTRODYNAMICS OF THE POLAR CAP

In the reference frame corotating with the NS the Gauss law is (see e.g. Arons & Scharlemann 1979)

$$\nabla \times E = 4\pi(\eta - \eta_{\text{GJ}}) \,. \tag{A1}$$

In the 1D approximation the only changing component of electromagnetic fields is the electric field parallel to the static magnetic field of the NS. The solution of equation (A1) is given by

$$E = E|_{x=0} + 4\pi \int_0^x (\eta - \eta_{\text{GJ}}) \, ds \,. \tag{A2}$$

I am solving a non-stationary problem where boundary conditions can change with time because the magnetosphere can respond to the changes of conditions in the polar cap. If the electric field just outside the NS surface $E|_{x=0}$ is known at any given moment of time, the electric field in the calculation domain can be calculated using equation (A2). For this problem it is more convenient to reformulate the boundary conditions on the electric field at the NS surface $E|_{x=0}$ in terms of the electric current flowing through the system.

As η_{GJ} does not change with time, differentiating equation (A2) with respect of time and using charge conservation

$$\frac{\partial \eta}{\partial t} + \frac{\partial j}{\partial x} = 0 \tag{A3}$$

I get

$$\frac{\partial E}{\partial t} = \left. \frac{\partial E}{\partial t} \right|_{x=0} - 4\pi(j - j|_{x=0}) \,, \tag{A4}$$

or

$$\frac{\partial E}{\partial t} = -4\pi(j - j_{\text{m}}) \,, \tag{A5}$$

where

$$j_{\text{m}} \equiv \frac{1}{4\pi} \left. \frac{\partial E}{\partial t} \right|_{x=0} + j|_{x=0} \,. \tag{A6}$$

To clarify the meaning of j_{m} let us consider a small region at the NS surface (see Fig. A1). NS crust can be considered as a good
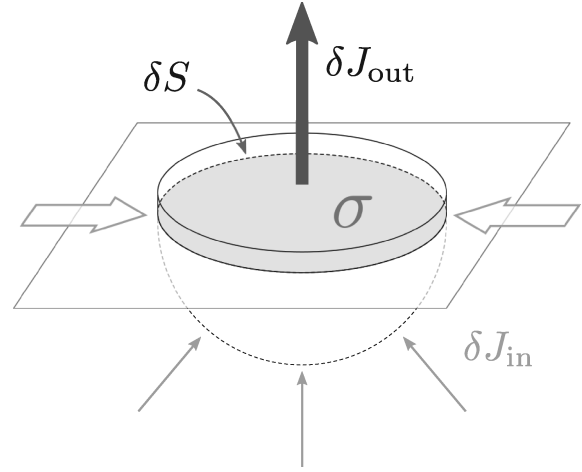

Figure A1. Current flow through the surface on the NS (see text for explanation).

conductor; the charges can accumulate only on its surface, and the electric field in the crust is zero. The electric field at the NS surface $E|_{x=0} = 4\pi\sigma$, where σ is the surface charge density. The change of the total charge in the fiducial volume in Fig. A1 δq is due to currents through the boundaries of the volume:

$$\delta q = \delta\sigma\,\delta S = \delta t(-\delta J_{\text{out}} + \delta J_{\text{in}}) = \delta t(-j|_{x=0}\,\delta S + \delta J_{\text{in}}) \,. \tag{A7}$$

For the electric field at the NS surface I have then

$$\frac{1}{4\pi} \left. \frac{\partial E}{\partial t} \right|_{x=0} = \frac{\partial\sigma}{\partial t} = -j|_{x=0} + \frac{dJ_{\text{in}}}{dS} \,. \tag{A8}$$

Substituting this expression into equation (A6) I get

$$j_{\text{m}} = \frac{dJ_{\text{in}}}{dS} \,, \tag{A9}$$

i.e. j_{m} is the current density which flows in the NS crust towards the discharge zone; it causes current in the discharge zone and/or accumulation of charges at the NS surface. In other words, j_{m} is the current density that the magnetosphere wants to flow through the cascade zone. Equation (A5) is a convenient form for an equation for the electric field in a problem where a large system with very high inductivity requires some specific current density from a much smaller system plugged into the same electrical circuit (see e.g. Levinson et al. 2005; Beloborodov & Thompson 2007). Note that equation (A5) correctly accounts for the retardation of changes in the electric field – at any given point in space the electric field changes if j deviates from j_{m}; the current density j is generated by particle motion, and the latter cannot move faster than the speed of light.

This paper has been typeset from a TeX/LaTeX file prepared by the author.